SAND REPORT

SAND2004-6437
Unlimited Release
Printed December 2004

Meso-scale Controlled Motion for a Microfluidic Drop Ejector

Paul Galambos, Gil Benavides, Mark Braithwaite, Clint Atwood, Rick Givler, David Luck, Ken Pohl, and Dave Czaplewski

Prepared by
Sandia National Laboratories
Albuquerque, New Mexico 87185 and Livermore, California 94550

Sandia is a multiprogram laboratory operated by Sandia Corporation,

a Lockheed Martin Company, for the United States Department of Energy's National Nuclear Security Administration under Contract DE-AC04-94-AL85000.

Issued by Sandia National Laboratories, operated for the United States Department of Energy by Sandia Corporation.

Available to DOE and DOE contractors from
U.S. Department of Energy
Office of Scientific and Technical Information
P.O. Box 62
Oak Ridge, TN 37831

Telephone: (865)576-8401
Facsimile: (865)576-5728
E-Mail: reports@adonis.osti.gov
Online ordering: http://www.doe.gov/bridge

Available to the public from
U.S. Department of Commerce
National Technical Information Service
5285 Port Royal Rd
Springfield, VA 22161

Telephone: (800)553-6847
Facsimile: (703)605-6900
E-Mail: orders@ntis.fedworld.gov
Online order: http://www.ntis.gov/help/ordermethods.asp?loc=7-4-0#online

SAND 2004-6437
Unlimited Release
Printed December 2004

Meso-scale Controlled Motion for a Microfluidic Drop Ejector

Paul Galambos, Gil Benavides, Mark Braithwaite, Clint Atwood, Rick Givler,
David Luck, Ken Pohl, and Dave Czaplewski
Organizations: 1769, 14132, 14153, 9114, 1112

Sandia National Laboratories
P.O. Box 5800
Albuquerque, New Mexico 87185-1080

Abstract

The objective of this LDRD was to develop a uniquely capable, novel droplet solution based manufacturing system built around a new MEMS drop ejector. The development all the working subsystems required was completed, leaving the integration of these subsystems into a working prototype still to left to accomplish. This LDRD report will focus on the three main subsystems: (1) MEMS drop ejector—the MEMS 'sideshooter' effectively ejected 0.25 pl drops at 10 m/s, (2) packaging—a compact ejector package based on a modified EMDIP (Electro-Microfluidic Dual In-line Package---SAND2002-1941) was fabricated, and (3) a vision/stage system allowing precise ejector package positioning in 3 dimensions above a target was developed.

Acknowledgements:

We, the authors would like to acknowledge the support and work of several people on this project and apologize in advance to anyone we may have inadvertently slighted by leaving off or including in this acknowledgment. Sita Mani was very helpful in this project especially in fabricating a specially processed SUMMiT^{TM} wafer with Poly4 replace by silicon nitride, allowing us to see how our devices filled with liquid. Amanda Lopez and Jaime Reif helped package and test ejectors. Bernie Jokiel produced the 1st ejector designs. Guy Prevost was instrumental in the vision system development, and Randy Shul and Sarah Rich accomplished the two-step Bosch etch process required by these devices. Finally, the authors would like to thank the Advanced Manufacturing LDRD committee for funding this effort and the Microelectronics Development Lab (MDL) staff and operators for making the MEMS ejectors. Sandia is a multi-program laboratory operated by Sandia Corporation, a Lockheed Martin Company, for the United States Department of Energy's National Nuclear Security Administration under contract DE-AC04-94AL85000.

Intentionally Left Blank

TABLE OF CONTENTS

Introduction

The goal of this LDRD was to produce a working MEMS (Micro-Electro-Mechancal Systems) 'sideshooter' ejector patterning system. The primary application addressed by this system is micro-nano scale fabrication of 'wet' systems and devices. There are many other applications for droplet patterning systems that range from well established but still evolving (ink-jet printing [1]) to more revolutionary with a longer term payoff (writing organic electronic circuits [2]). More potential applications include: dispersal of medicine [3], spot arrays [4], mass spectroscopy [5], adhesives application and 3D plastic prototyping [6], and coatings (e.g. for sensors) [7], – to name a few.

Micro-nano scale fabrication of 'wet' systems and devices should enable new applications relating to unique functional nano, bio or bio-inspired surfaces that are simultaneously patterned for specific tasks across a wide range of scales, from the nanometer scale (molecules) to the micrometer scale (microfabrication) to the millimeter scale (engineered material systems). Layer by layer deposition via drop ejection can result in the buildup up these patterned nano-materials into tissue-like 3D structures with significantly greater capabilities than the 2D layers. This bio-like structure can be fabricated by processes under our control and does not require the significant time needed for mediated bio-material growth. Other potential micro-nano scale fabrication techniques (e.g. high vacuum lithography) are not as compatible with 'wet' systems and therefore are not useful for bio-surface or organic wet-chemistry nano-fabrication. Therefore the manufacturing capability we aimed to develop in this LDRD can be viewed as a disruptive technology that will enable as yet unimagined nano-micro scale systems with new capabilities.

The possibilities of nano-micrometer scaled droplet produced surfaces are explored by Fan, Brinker et. al [8] as they pertain to evaporative-induced self-assembly (EISA) of molecular-scale structures into organically modified patterned meso-phases via printing procedures. This paper provides clues to the capabilities our fabrication system will require. In [8] functional organic moieties are positioned on surfaces of pores that are organized into networks that provide size selective accessibility to liquids or gases. These pore networks are organized on a larger scale into 1D and 2D fluidic or photonic systems. Stable homogeneous inks that on evaporation undergo self-assembly to form the desired organically modified silca-surfactant meso-phases (pore networks) were prepared using oligomeric silica sols in ethanol/water solvents. Preferential evaporation of ethanol causes enrichment of water, surfactant and silicates, establishing a gradient in their respective concentrations. When the critical micelle concentration is exceeded, micelles form and are organized into mesophases on further evaporation. Even further evaporation results in the pores assembling into networks with the organic molecules attached to the pore support surface and a very open silica supported pore structure. Such a structure has potential sensor, display and optical wave-guide applications (see [8] for more details).

While there are a number of groups interested in droplet based fabrication and there is even a company making its living in this area (www.microfab.com – fabricates micro-lenses and other devices via drop ejection) none of the fabrication systems yet developed address all the important capabilities required for of a truly disruptive nano-micro fabrication technology such as we are trying to develop. In addition, existing droplet fabrication machines are typically very large (room scale) and are not taking advantage of the possibilities of MEMS and meso-scale packaging methods to reduce the volumes of fluid required and increase system integration with the associated batch production, power and scale advantages.

A useful disruptive drop ejection fabrication microsystem capable of nano-microscale wet surface patterning of bio-materials would ideally have the following capabilities (as would be useful to create devices such as those described in [8] and other potential devices and systems):

1) Drop size. Small drop size allows for small feature size definition. A one micron diameter drop is approximately one femtoliter in volume and even smaller drops are theoretically possible. One can possibly get below the photolithographic feature size limit of approximately one micron.

2) Variable drop size. One can perhaps adjust the drop size on demand to allow for rapid deposition of different sized drops at different locations on a surface allowing such applications as fluid or optical focusing to a very small scale along a deposited feature.

(3) Line printing vs. drop printing. In certain patterns a line is desirable and in others individual drops are desirable. A series of adjacent drops approximates a line to a certain degree. It may be desirable to have a line printing ejector nozzle and a spot printing ejector nozzle on the same MEMS ejector head.

(4) Ejection of different materials. Precise interface definition between two different ejected drops is valuable because much of the chemistry of interest and self-assembly occurs at interfaces between materials and phases. By ejecting different material solutions from adjacent or nearby ejector nozzles and having the drops impinge adjacent to each other at a precise location (either by controlling drop flight direction or by moving the target stage) precise and very small scale patterns of interfaces can be generated.

(5) Drop velocity. Variation in drop velocity can result in variation in the amount of drying that occurs and the shape of the impacting drop on the target surface.

(6) Drop ejection frequency. Ideally one would like very high frequency ejector operation to increase the speed at which a pattern can be produced.

(7) Drop location precision. Not only does one want a very small drop, but one wants drop precision to be controlled to at least the level of the drop size.

(8) Mix-then-eject. Many solutions react when they are mixed. By putting two different solutions together and then immediately ejecting the mixture volatile, unstable or very rapidly reacting solutions can be deposited and patterned. The mix-then-eject capability can be accomplished with very small volumes by using integrated on-chip valves and pumps to bring two or more solutions together in the ejection chamber immediately prior to drop ejection.

(9) Other effects – mechanical drop ejection can be combined with heat, E-field or other effects if so desired as these fields can be built into the MEMS device. However, such fields are not required as they are in thermal or electro-spray ejection techniques. Such fields may be destructive to solutions of interest.

(10) Layers. The ability to rapidly lay down layers of droplet patterns allows 3D fabrication.

(11) Cells, particles, bubbles. The ability to eject cells, solids (e.g. beads) or trapped gases (bubbles) onto a surface provides additional functionality.

(12) Target surface patterning before drop ejection onto the surface allows more pattern control as, for instance, in the fabrication of hydrophobic and hydrophilic surface patterns on which drops are deposited.

(13) Liquid feed to the target from below or the side allows one to keep the surface that has been deposited wet, or portions of the surface to be maintained wet if so desired in a particular application.

Our goal on this LDRD was to develop a drop-ejection fabrication microsystem with the capabilities listed above or at least a reasonable development path to these capabilities. The rest of this report will be devoted to describing just how much progress was made towards developing the drop ejection fabrication microsystem in the areas of: (1) MEMS ‘sideshooter’ drop ejector development (design, fabrication, and testing), (2) packaging of the ejector, and (3) the vision and stage system developed to enable precise patterning of surfaces with the packaged MEMS drop ejector.

MEMS Sideshooter Ejector

The MEMS 'sideshooter' refers to the fact that in this ejector concept a surface micromachined piston is electrostatically actuated horizontally into a chamber filled with liquid that has a hole in the top so that the drop is ejected vertically. The ejector nozzle is in the top nozzle plate while the piston actuates into the side of the chamber. The drop is ejected out of the nozzle at a 90 degree angle to the piston motion – hence a 'sideshooter' (see Figs. 1 and 2).

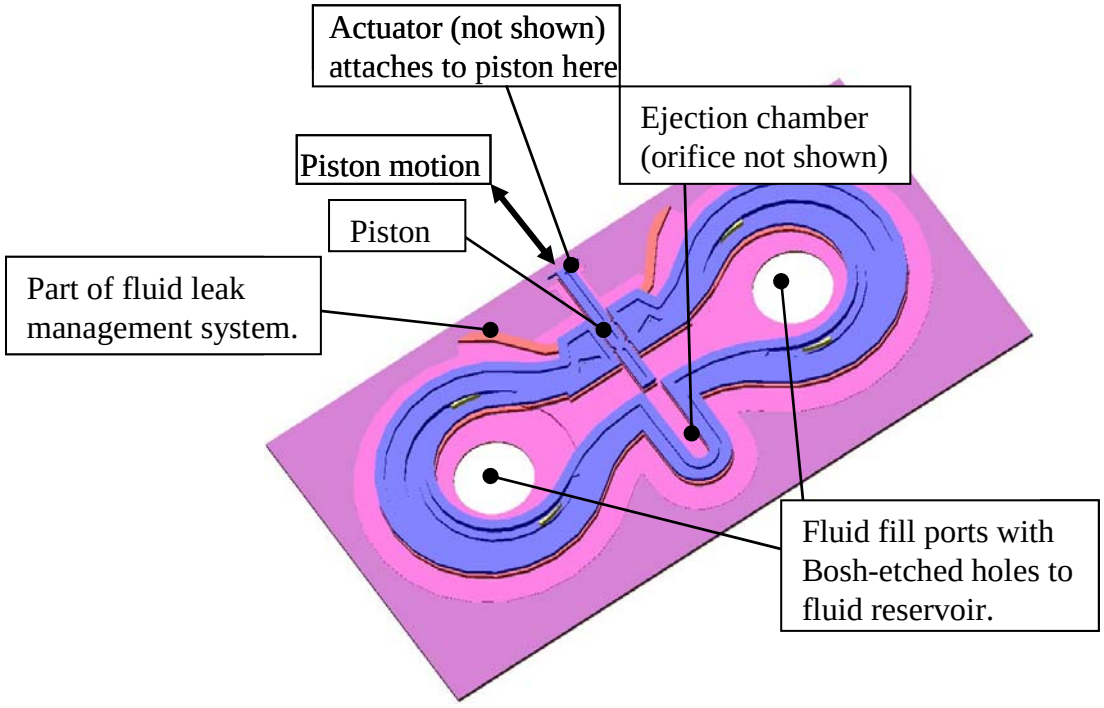

Figure 1a. SUMMiT™ Sideshooter Ejector Concept. Nozzle plate removed and actuator not shown.

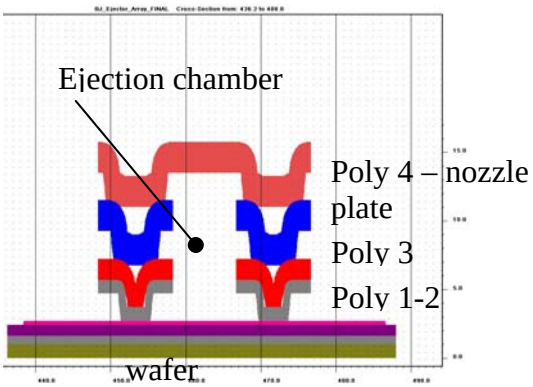

Figure 1b. Ejection chamber cross-section. The walls are formed by Poly (polysilicon) layers 1-2 and 3. Nozzle plate cover formed by Poly 4. Total height of chamber is approximately 8.5 microns.

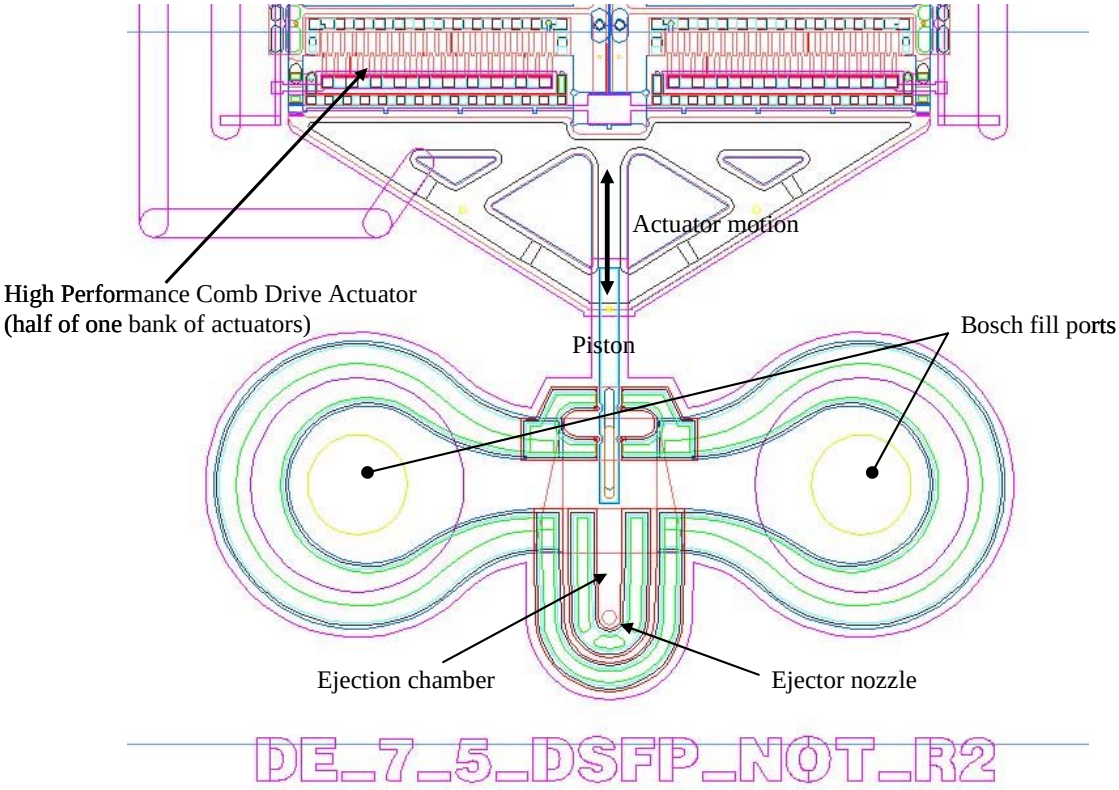

Top view – AutoCAD design

Figure 1c. AutoCAD design of sideshooter ejector. The High Performance Comb Drive Actuator (HPCD) drives the piston into the ejection chamber to eject a drop out of the top ejector nozzle.

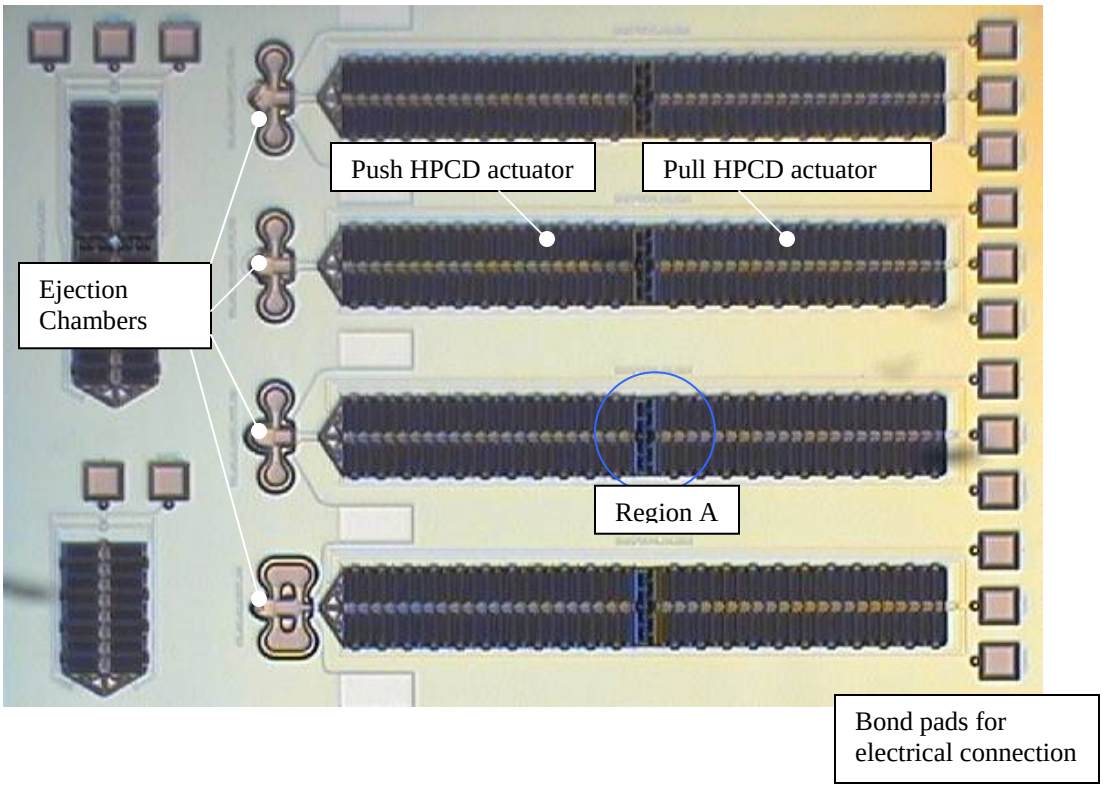

Figure 2a. As fabricated first generation sideshooter ejector. Module 4 RS349. Each module fabricated contains multiple ejector design variations.

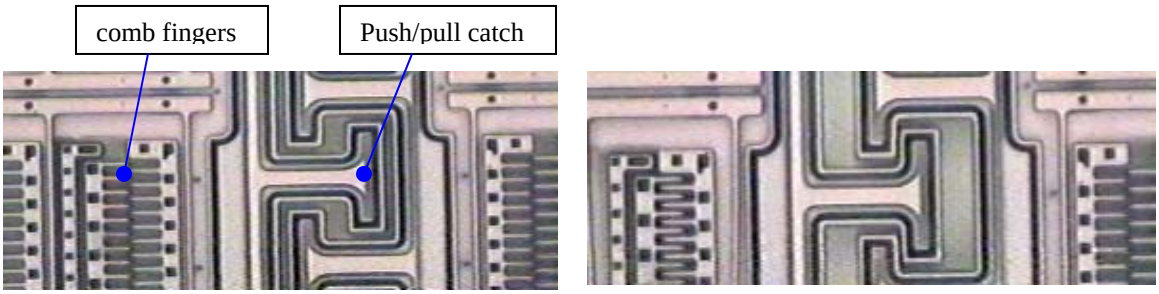

(b) (c)

Figure 2b,c. Actuator detail of region A above (Figure 2a). No voltage applied (left image Fig. 2b) – comb fingers apart and push/pull catch not engaged. Voltage applied to left (push) actuator to drive the piston into the ejection chamber (right image Fig. 2c) – comb fingers together and push/pull catch engaged. At this point the pull actuator can be powered to rapidly pull the piston back out of the ejection chamber for rapid chamber refill and drop size control.

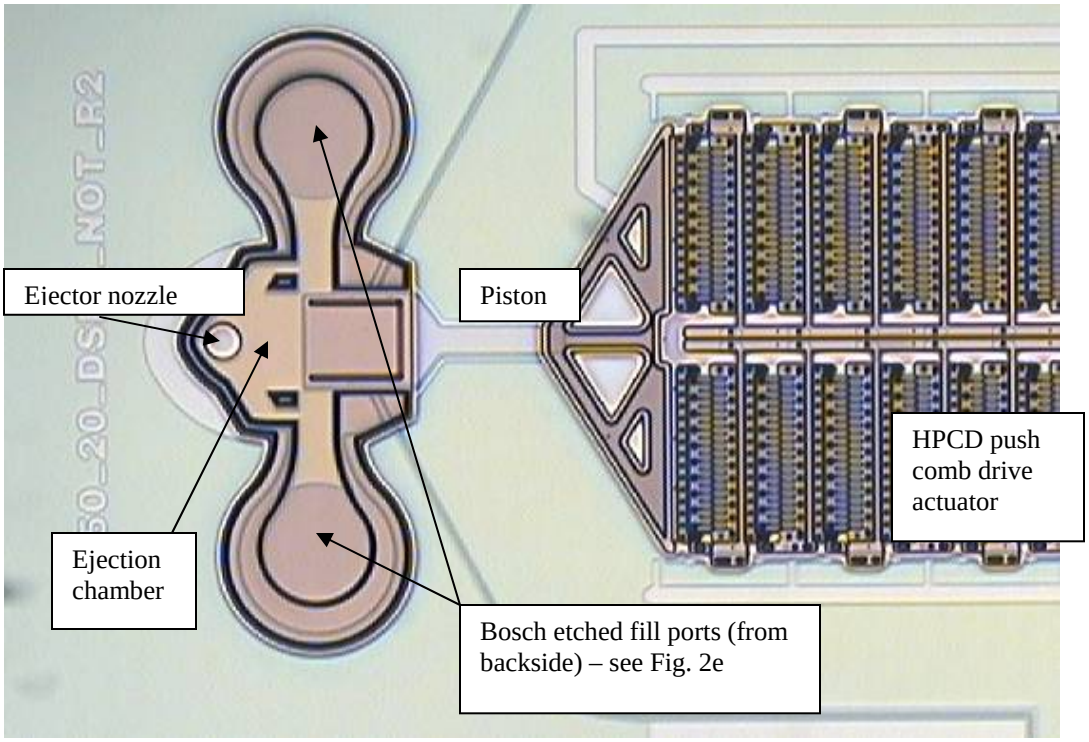

Figure 2d. Close-up of ejection chamber.

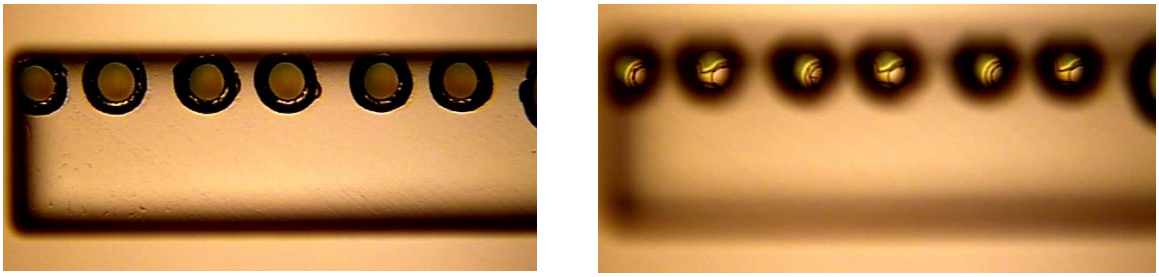

(e) (f)

Figure 2e,f. Backside of ejector MEMS die showing Bosch-etched [14] liquid feed connections to fill ejection chamber fill ports. Fig. 2e image focus is on the large counterbore that allows liquid feed to many ejection chambers at once. Fig. 2f image focus is through the wafer to the front surface where part of the ejection chamber feed port sidewall is visible.

Comparison with other Ejection Methods

The mechanism of drop formation and ejection is entirely mechanical – unlike a thermal ink jet which effectively boils liquid drops out a nozzle – and there is no electric field applied across the 'ink' unlike the electrostatically actuated 'roofshooter' that we previously developed [9]. These factors make the sideshooter much more insensitive to the properties of the liquid being ejected than either of these methods as neither the thermal properties (heat capacity, thermal conductivity, boiling temperature) nor the electrical properties (dielectric constant, breakdown voltage, electrolysis limits) of the liquid are important to device operation. The only liquid properties that effect drop ejection in the sideshooter are viscosity and surface tension. The effects of either mechanical property can be compensated for by varying the actuator drive signal (changing the driving force of the piston) or if that is insufficient designing in a higher force actuator (for the case where a very high viscosity fluid must be ejected). Also the fact that no significant temperature change is induced in the liquid during drop ejection reduces any potential phase change or denaturing effects such as could affect the EISA deposition of [8]. If, however, one desires either heating of the liquid or electric field application during drop ejection it could be designed into the ejection chamber simply by attaching an electrical trace to a heating or charging pad in the ejection chamber. This secondary effect would be independent of the mechanism of drop ejection and therefore could be varied through a wide parameter space.

The sideshooter ejector concept also has potential advantages over the other main established ejection method - piezoelectric drop ejectors. Piezoelectric ejection systems rely on the deformation of a piezoelectric crystal when a voltage is applied to drive a drop out of a nozzle orifice. Piezoelectric deflections are typically very small (microstrain deformations [10]) so they are operated at resonance with the ejector chamber tuned to the transducer. The relatively large liquid volume required for piezoelectric drop ejection as compared to our MEMS sideshooter ejector is not only wasteful of potentially expensive or hard to synthesize chemicals, but also inhibits any mix-then-eject applications because such a relatively large volume must be mixed with the resulting large mixing times required – effectively eliminating piezoelectric actuation as an option for mix-then-eject applications.

The carefully tuned ejection chamber required for piezoelectric drop ejection is generally capable of one size and one velocity drop ejection only. For the application discussed in the introduction we would like to be able to vary drop size, drop velocity and precise drop position 'on-the-fly' – a capability that is beyond the scope of a typical piezo-electric ejector, but which the sideshooter can potentially address. Since the sideshooter ejector piston stroke length and velocity can be adjusted independently simply by changing the drive signal, it should be possible to eject drops over a range of drop diameters and drop velocities from the same orifice. Also, since the sideshooter imparts a horizontal velocity to the drop (see Fig. 3) the precise point of drop impingement can be at least theoretically controlled – also with drive signal variation.

The piezoelectric crystal is a different material than the main body of the ejection chamber so it typically must be glued in place onto a somewhat flexible wall of the ejection chamber. This assembly process can be complicated and there can be significant variation from assembly to assembly, leading to carefully controlled process requirements and potentially a higher cost than with the monolithic MEMS ejection system that we are developing.

All of these potential advantages of our MEMS sideshooter ejector are offset by the disadvantage of our sideshooter being a disruptive technology that is not yet in existence, while these other ejection systems are already commercially available. In certain applications the advantages of our system may result in capability that is impossible with commercial ejection systems, making our system necessary for these new capability applications. These applications should drive further development of the 'sideshooter' MEMS ejector patterning system described in this report.

Ejector Design

The design of the sideshooter separates the actuator mechanism from the ejection chamber. Different actuators can be coupled to the same ejection chamber design by changing the MEMS design of the actuator. In this manner many different parametric variations can be incorporated onto the same prototype MEMS module. Four prototype MEMS ejector modules were designed and fabricated. A 1st generation SUMMiT™ (www.sandia.gov/micromachine) ejector module was tested and results from this testing were used to redesign the sideshooter. Two new SUMMiT™ modules were designed as well as a SwIFT™ (SUMMiT™ with additional silicon nitride layers allowing transparent microfluidic channels with embedded electrodes or heater to be fabricated) ejector module. The SwIFT™ designs will allow us to see inside the ejection chamber during the ejection process and perhaps perform PIV (Particle Image Velocimetry) to measure detailed flow patterns during drop ejection. One of the 2nd generation SUMMiT™ ejector designs was thoroughly tested and successfully ejected 8 micron diameter drops (see results section). The parametric design variations incorporated into the 2nd generation MEMS ejector design that was tested (RS424, module 8) are summarized in table 1 below. Other parametric variations were designed into other design modules and are not discussed in this report.

Table 1. 2nd Sideshooter Ejector Parametric Variations:

List of parameters:

1) Number of actuator banks (11 or 21/22 banks). [2 variations]
2) ~10 micron or ~6 micron actuator travel. [2 variations] The first 2 μm of the piston stroke are used to cut-off the ejection chamber fill path, therefore the effective stroke length for ejection is 2 μm less than the designed piston stroke.
3) Actuator piston width (depends on actuator travel and nozzle diameter). [3 widths possible (but not necessarily used) per travel length and ejector nozzle diameter – base, wide, narrow]. Width of 10 micron width for 2 and 5 micron diameter ejector nozzles. Nominal width of 50 microns for 10 micron ejector nozzle diameter with a wide piston of 75 microns and a narrow piston of 35 microns. Width of 100 microns for 15 micron diameter nozzle and widths of 150 and 300 microns for 20 micron diameter nozzle.
4) Ejector nozzle diameter (2, 5, 10, 15, and 20 micron diameter). [5 variations in diameter] There are also two locations for the nozzle. Most designs have the nozzle near the end of the ejection chamber opposite the piston, however a few designs had a centered ejection chamber nozzle – including the design which we had the most success filling and ejecting drops from.
5) Bleed configurations (no bleed, 100% bleed – bleed area as % of nozzle area). [2 variations]
6) Fill path - see discussion on ejector filling below.
7) Piston shaft sealing configuration – baseline seal around rectangular piston shaft consists of dimples to restrict flow followed by a sudden sidewall expansion seal and a nitride cut wick or Poly 1-2 blocking wall beneath the piston shaft (see Fig. 4).

As highlighted in the table two key variations in ejector design are explored parametrically; actuator stroke and force per volt, and the leak seal around the piston. There are other design variations worth pointing out – such as the nozzle diameter and the Bosch etch configuration – but the most important parameters are concerned with the actuator and the piston seal.

Actuator Design - Forces

The chief functions of the actuator are to deliver the force required at the rate required for drop ejection. In order to eject a drop the piston actuators must be able to produce enough force to push the piston rapidly (~1 m/s) into the ejection chamber and accelerate (~5 microseconds to full velocity) the drop out of the nozzle at approximately 10 m/s. The piston is typically larger in area than the nozzle. Therefore by conservation of mass the piston can produce a drop velocity that is larger than the piston velocity by approximately the ratio of piston area to nozzle area. This does not take any leakage around the piston into account which will reduce the amount of liquid going out the nozzle.

In addition to overcoming inertia to accelerate the drop, the electrostatic HPCD actuator must provide enough additional force to overcome friction, viscous drag as the piston pushes through the liquid surrounding it, actuator spring force (acting to return the piston to it's as fabricated position when the voltage is turned off), and surface tension associated with creating new liquid surfaces.

First consider the electrostatic HPCD force. The electrostatic force can be calculated from the equation for fringe field comb drives:

$$F_{ES} = \left[\frac{n \cdot \varepsilon \cdot t}{g}\right] \cdot V^2 \qquad \text{Eqn. (1)}$$

where n is the number of comb fingers, ε is the dielectric constant for fluid between comb fingers (in this case air - $\varepsilon = 8.854 \times 10^{-12}$ C/V-m), t is the thickness of the comb finger, g is the gap between moving and stationary comb fingers (typically moving comb is at ground and fixed comb is at applied voltage), and V is applied voltage. The HPCD is fabricated in banks of 4 combs per bank that are added together to give a larger force. For instance the HPCD shown in Fig. 2a has 11 actuator banks set to actuate in the push mode and 11 actuator banks set to actuate in the pull mode. In Fig 2d three actuator banks are shown. The ejector which we successfully tested had 21 banks operating in the push mode to drive the piston into the ejection chamber. The device ejected drops at V = 80V. There were 20 fingers per comb or 80 fingers per bank (n=80), the thickness was t=6.75 μm, and the gap between opposing charged teeth was g = 0.5 μm. Therefore,

$$F_{ES} = \left[\frac{n \cdot \varepsilon \cdot t}{g}\right] \cdot V^2 = \left[\frac{80 \cdot 8.854 \times 10^{-12} \cdot 6.75 \times 10^{-6}}{0.5 \times 10^{-6}}\right] \cdot 80^2 \approx 61\,\mu N \text{ or } 0.061\,mN$$

per 4 comb actuator bank, and the 21 bank actuator produces 21 x 0.061 = 1.28 mN of electrostatic (ES) force at V=80V (approximately 1250 μN). In [11] a larger force of 2.5 mN was produced for an even longer (more banks of combs) actuator at V=100V.

Part of this actuator force is used to deform the return spring that pulls the piston back and allows the ejection chamber to refill once the voltage signal is turned off. The dry DC voltage actuation test gives the distance the piston actuator is moved and therefore the deflection of the return springs for a given voltage. It took roughly 30V to achieve approximately 3 μm of deflection with the 21 bank actuator so the spring force was approximately F_{sp} = 0.18 mN (using Eqn 1) and the spring constant of the return spring is approximately:

$$F_{sp} = k \cdot x,\ k = \frac{F_{sp}}{x} = \frac{180\ \mu N}{3\ \mu m} = 60\ \mu N / \mu m \qquad \text{Eqn (2)}$$

Since to eject a drop the piston must travel 4.5 μm the spring force overcome is (4.5/3.0) x 60 = 90 μN (approximately 100 μN – about 1 ½ of the 21 banks are supplying the force to overcome the spring force).

In order to determine the forces required to overcome fluid resistance and eject a drop we utilized a GOMA analysis from Rick Givler (dept. 9114). GOMA is Sandia's internally developed incompressible fluid mechanics code that is able to handle liquid/solid and liquid/gas, surface tension dominated, interactions

[12]. A 2D slot ejector was assumed in order to avoid having to solve the full 3D flow-field but still provide guidance as to the force required for drop ejection. At the time of this analysis the code was not able to model the break-off of the drop, so it must be inferred from the necking observed at the base of the (see Fig 3b and 3c below). The drop meniscus was pinned at the edge of the nozzle hole eliminating the possibility of leakage onto the front surface of the nozzle. This is a reasonable assumption for rapidly applied piston actuation with a hydrophobic front nozzle surface.

Figure 3 shows the results from this analysis. The width of the 2D slot out of which the drop is ejected is 5 μm and the channel depth is 8 μm with a 1 μm gap between the piston and each channel wall to give a 6 μm plunger (piston). The plunger is shown as the outlined rectangle inside the channel. The piston position at each time at which velocity contours are shown gives some indication of the piston motion and velocity. The color contours indicate velocity in cm/s. The liquid properties are surface tension σ = 30 dynes/cm (0.03 N/m), viscosity μ = 3.0 centipoise ($3x10^{-3}$ N-s/m^2), and density ρ = 1.0 gm/cc (1000 kg/m^3). This corresponds to liquid with the density of water, 3 times the viscosity of water and about ½ the surface tension of water.

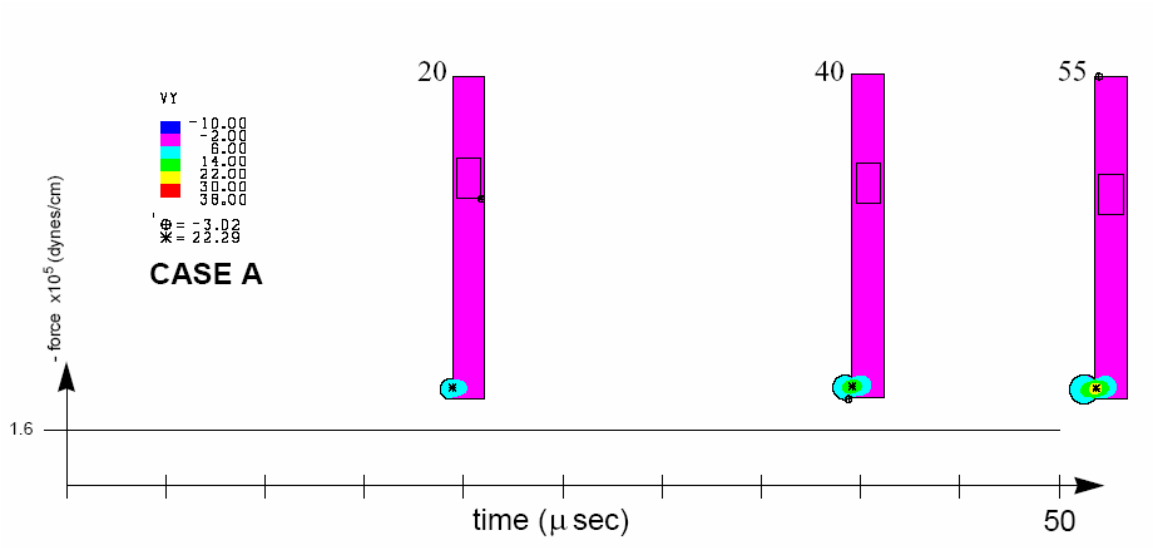

Figure 3a. Drop bulges but does eject at 1.6 x 10^5 dyne/cm (160 N/m).

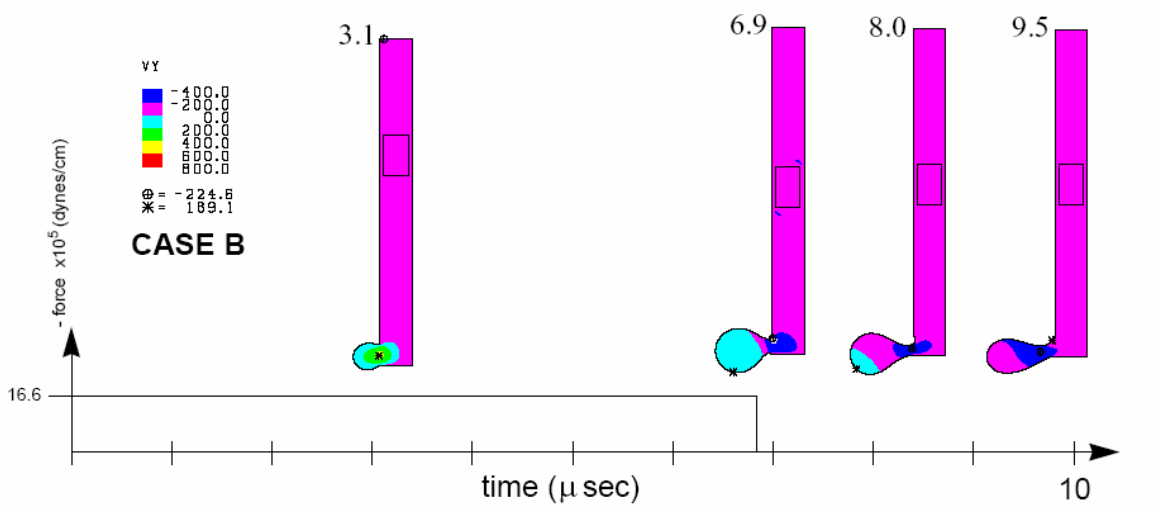

Figure 3b. Borderline drop ejection/no ejection at 16.6 x 10^5 dynes/cm (1660 N/m).

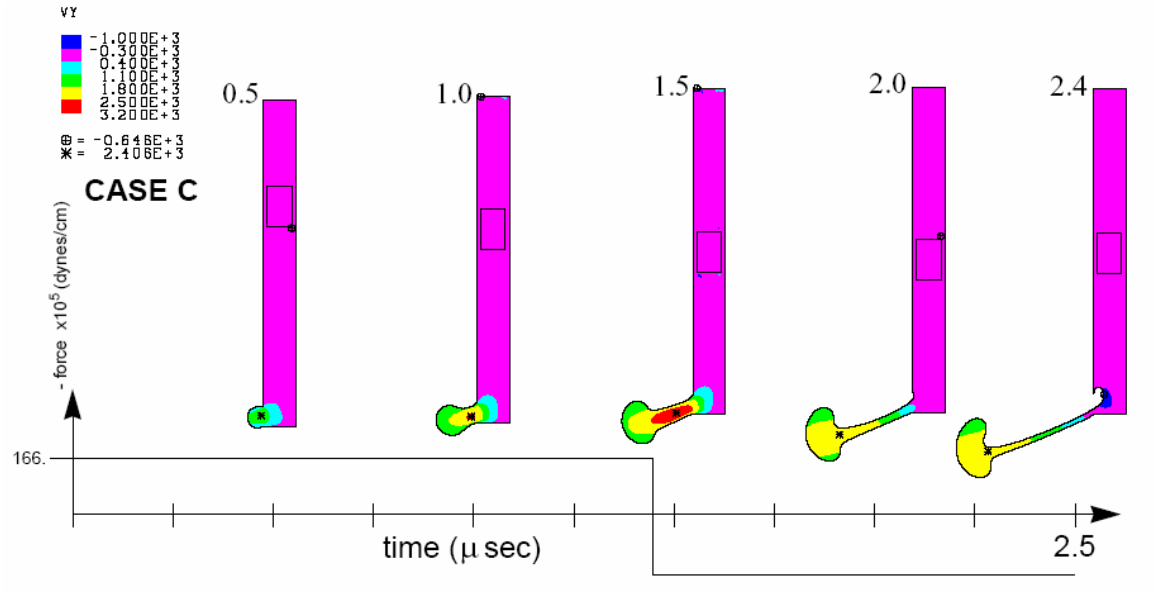

Figure 3c. Strong drop ejection at 166x10^5 dyne/cm (1.66x10^4 N/m) with sudden reversal of force direction at ~1.5 μs to assist drop break-off.

To compare a slot analysis to a round nozzle one needs to determine and appropriate slot width. Consider matching the Weber number for the slot geometry with the Weber number for the slot geometry. Weber number (We) is the non-dimensional ratio of inertia forces to surface tension forces and can be calculated from:

$$We = \frac{\rho \cdot V^2 \cdot l}{\sigma} \qquad \text{Eqn. (3)}$$

Where ρ is density, V is velocity, σ is surface tension and l is the wetted perimeter of the nozzle hole or slot. A typical condition for ejection with a 5 μm diameter nozzle ($l = \pi$ D = 1.57 x 10^{-5} m) with water (σ = 0.073 N/m, ρ =1000 kg/m^3) and V = 10 m/s is:

$$We = \frac{10^3 \cdot 10^2 \cdot 1.57 \times 10^{-5}}{0.073} = 21.5$$

From previous analyses of drop ejectors [13] it is known that this magnitude We should produce a drop, but not really strong ejection (borderline ejection). The velocity contours from Fig 3b actually show drop velocity <5 m/s, so the borderline ejection analysis of Fig. 3b is borderline but not quite ejecting a drop. Slightly more drop velocity and deformation than developed in Fig. 3b should result in drop ejection at a We of approximately 20. The strong ejection shown in Fig. 3c shows drop velocities of 25 m/s and a corresponding We = 50.

By matching the wetted perimeter (l) of the fabricated circular nozzle with the perimeter resulting from specifying a slot width in the above analysis, a matching Weber number and similar drop ejection should result. To match perimeters:

$$w = \frac{\pi \cdot D}{2} = \frac{\pi \cdot 5 \times 10^{-6}}{2} = 7.85 \times 10^{-6}\ m$$

where w is the width of the slot that matches We, and D is the diameter of the ejector nozzle. There is an additional correction due to the fact that the fabricated piston is approximately 10 times as wide as the nozzle and therefore needs to move only about 1/10th the velocity as in the analysis for the same drop velocity and Weber number. The slot analytical solution above assumes the piston and the nozzle are the same width. To roughly account for this difference divide the force predicted by the analysis by 10 as reaching 1/10th the velocity will only require approximately 1/10th the force (as a rough estimate). Therefore the adjusted (correction factors applied) actuator force required to eject a drop based on the above borderline ejection slot analysis (Fig. 2b above) is:

$$F = (1660\ N/m) \cdot (7.85 \times 10^{-6}\ m) \cdot (1/10) = 1.3\ mN$$

The 21 bank ejector provides approximately this magnitude force. The analytical solution is for a fluid that has 3x the viscosity of water, so ejecting water should require less force. The bottom line from this analysis is that an ejector actuator needs to supply significant force (for a MEMS actuator), on the order of 1-2 mN in order to eject a drop. Higher force actuators should be able to eject drops with more viscous fluids, but our 1.28 mN, 21 bank, HPCD actuator should provide just sufficient force to eject a drop of water from a 5 μm diameter ejector nozzle. Increasing nozzle diameter increases l in the Weber number calculation and makes it easier to eject a drop. The surface to volume ratio is smaller for the larger diameter nozzle, so the drop develops a larger inertia while overcoming the same surface forces and hence is easier to eject. Therefore we should expect strong drop ejection for the larger 10 μm diameter ejector nozzle with the 21 bank HPCD actuator.

Ejection Chamber Design - Filling

Surface chemistry controls how these surface micromachined devices will fill: that is what pressure is required to fill the ejection chamber, and what seal geometry or technique will keep the devices from leaking during the initial liquid fill process or during actuation. The surface chemistry is determined by the MEMS drying process. There are two drying processes being used in the MDL – one results in hydrophilic surfaces and the other in hydrophobic surfaces.

The final step in the MEMS fabrication process is the release etch in which the sacrificial silicon dioxide (oxide) layers are removed in an HF (hydrofluoric) acid bath. After a sufficient time in the acid to remove the sacrificial oxide the bath is diluted with water followed by methanol and must then be dried. The two MEMS drying techniques commonly used in the MDL are supercritical carbon dioxide drying (SCCO2), and vapor self-assembled monolayer drying (VSAM). SCCO2 drying relies on taking conditions in the drying chamber above the critical point so that there is never a liquid/vapor interface that can lead to the pulling together of MEMS layers and adhesion of these layers (stiction) preventing device mechanical actuation. Liquid CO_2 is pumped into the drying chamber to displace the methanol followed by removal of the CO_2 above the critical point. As a result the SCCO2 dried surfaces are hydrophilic – contact angle 35 degrees.

The VSAM drying method starts with the SCCO2 method, but following CO_2 removal a precursor gas (FOTAS – tris(dimethylamino)silane) is pumped into the drying chamber and a monlayer is deposited on all the MEMS surfaces. As a result the VSAM surfaces are hydrophobic – contact angle 110 degrees.

The packaging required to deliver liquid to the devices in the test station is described in the ejector testing section below. A positive pressure is applied to bring liquid to the device package and through it to the MEMS ejector module using either a head pressure or pneumatically controlled pressure. It is not possible to use a vacuum to pull liquid through the device because then air will be drawn into the ejection chamber through the ejector nozzle and the gap between the piston shaft and the ejection chamber housing. After the manifold is completely filled with liquid a cutoff valve is closed so that the liquid has only one place to go – into the ejection chamber - by displacing the air in the chamber out the nozzle hole and the gap between the piston shaft and the ejection chamber (piston seal).

The application of positive pressure to move liquid into a small gap hydrophilic channel creates problems because as the liquid enters the hydrophilic channels its local pressure drops and liquid is drawn into the chamber (wicking phenomena). Since the filling pressure remains high during wicking there is a sudden surge in flow into the very small ejection chamber and liquid tends to leak out the nozzle and piston seal. The liquid can then be drawn back into the chamber with a vacuum, but if the leak is large enough liquid will reach the actuator comb fingers and cause them to short or deposit a film on the comb finger surfaces upon evaporation that interferes with actuation. Alternatively if one could reduce the filling pressure rapidly enough the leak could be prevented. This sudden pressure cut-back, however, proved to be very difficult to do rapidly enough in practice without an automated feedback controlled system.

The hydrophobic release MEMS ejectors are actually easier to fill without leaking because as liquid is forced into the small passages leading to the ejection chamber and into the ejection chamber itself the pressure required to overcome the flow resistance of the smaller passages increases. Therefore a gradually higher pressure is required to move liquid into the chamber and a slower final fill of the chamber results. In the hydrophobic case when liquid was seen at the nozzle, suddenly dropping the pressure to atmospheric – by cracking the fill bottle to induce a leak in the line upstream of the device - effectively stops a large leak from occurring and allows effective priming of the ejection chamber.

The ejector chamber fill passage design, nozzle size and placement, and piston seal can all have an effect on how the device seals. There were several different sealing geometries designed into the various variations on the 1st generation baseline design (see Fig. 1). The filling and sealing geometry that was

successful was on ejector design 1 on Module 8 of RS424. This successful seal and fill passage geometry is shown in Fig. 4 below.

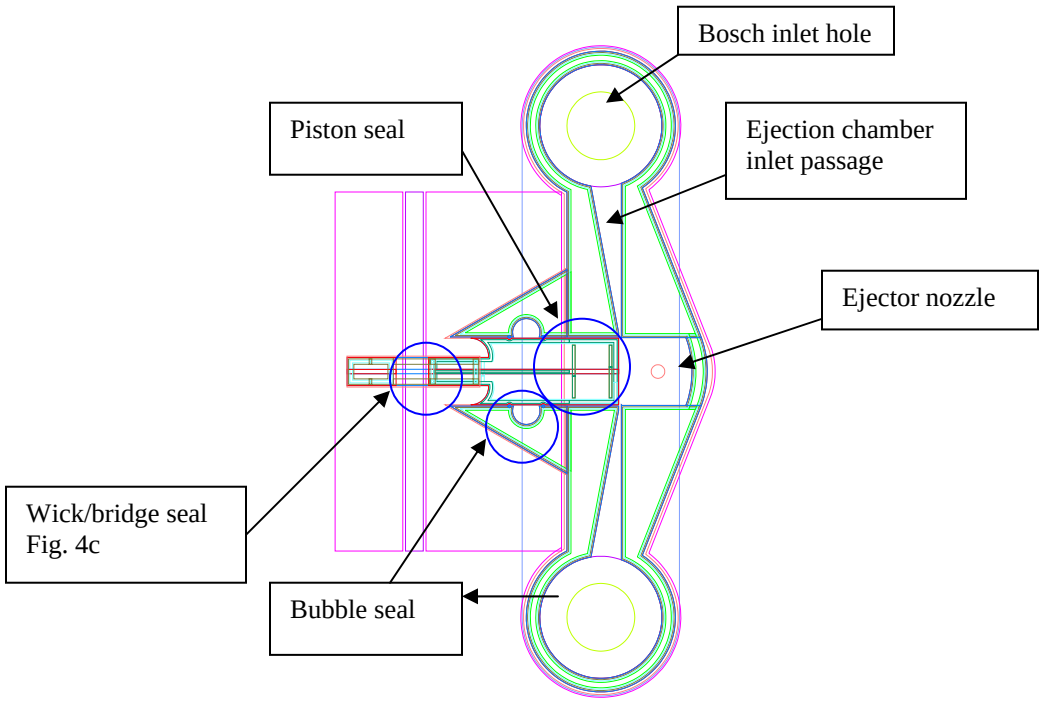

Figure 4a. Device 1 on Module 8 of RS424 – ACAC design of ejector. Actuator to the left not shown.

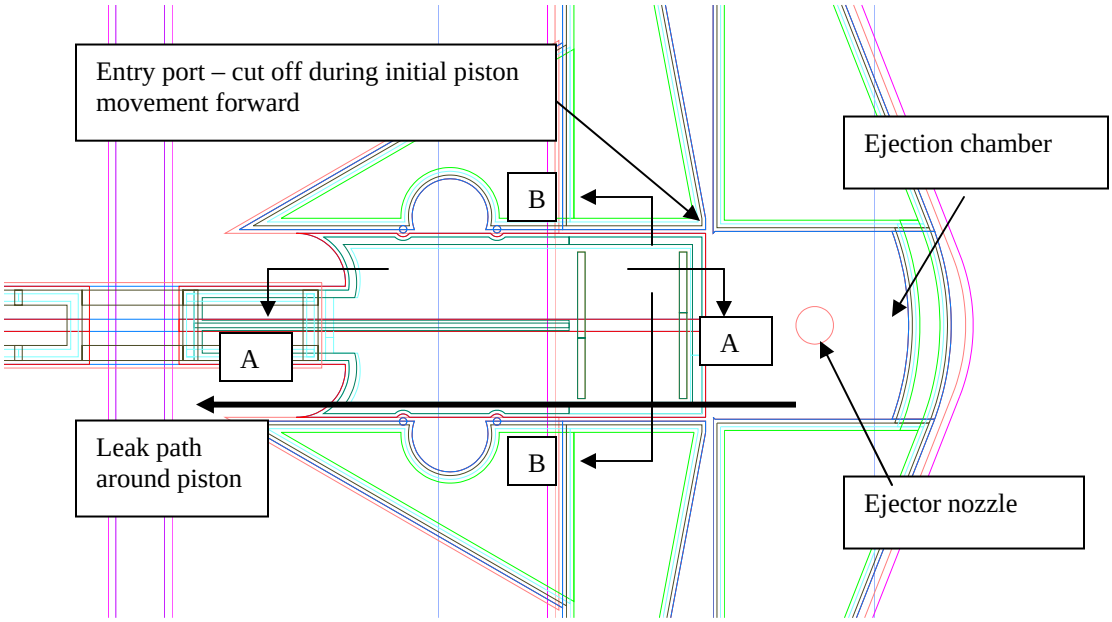

Figure 4b. Blow-up of ejection chamber.

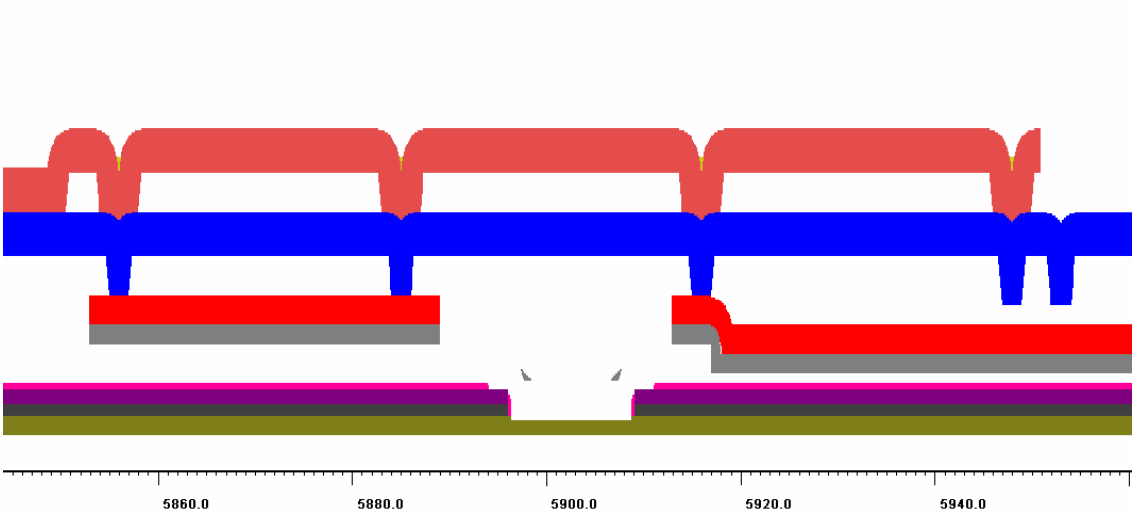

Figure 4c. Cross-section of wick/bridge seal.

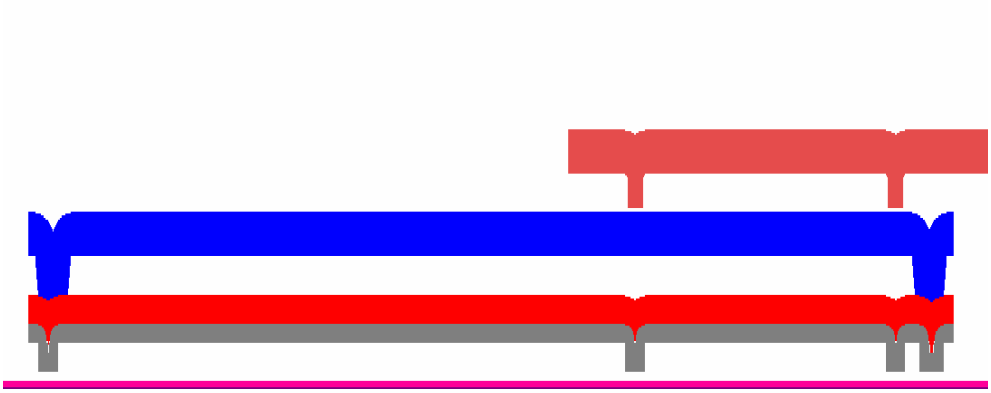

Figure 4d. Piston Seal (section A-A)

Figure 4e. Piston Seal (section B-B)

Liquid enters the ejection chamber through the Bosch-etched [14] through hole from the back of the wafer (Figs. 4a, 1a, 1c, 2d, 2e, 2f) and travels approximately 100 μm along the inlet passage (Fig. 4a) to the ejection chamber. The first 2 μm of the piston stroke are used to cut off the inlet passage and confine the pressurized region to just the ejection chamber (Fig. 4b). Liquid pushed forward by the piston then exits the top of the ejection chamber through the centered ejector nozzle (Fig. 4a and 4b). It is possible for liquid to leak around the piston and along the piston shaft. This is prevented though various sealing geometries. These seals include dimple region that reduce the gap between the moving piston and the stationary sidewall and reduce leakage by constricting the fluid flow (Figs. 4d and 4e), and a wick or moat-like structure (Fig. 4c - in some designs this is replaced by an Poly 1-2 blocking wall) beneath the piston shaft that directs liquid away from the actuator comb drives (not shown – to the left in Fig. 4a.). This particular geometry was effective in preventing liquid from leaking past the piston and wetting the comb drives. Other geometries were also investigated – especially on the first generation device module RS349 (fig. 2). A special fabrication run allowed us to replace the opaque top cover polysilicon layer with a transparent silicon nitride layer. The meant that we could see into the ejection chamber and observe the meniscus motion as the chamber filled (Figs. 10 to 15). Unfortunately this special run did not have the nozzle hole fabricated so no trapped air was able to exit from the nozzle hole. Therefore these images represent a worst case scenario for leaking, with the highest pressure at the piston gap that could result during device filling.

Ejector Testing

Special packaging (different from the patterning system package) was required to test the MEMS drop ejector in order to provide optical access at high magnification to the front of the ejector (nozzle view) for stroboscopic interrogation of the nozzle. In addition a filling flow manifold with upstream and downstream pressure and vacuum control was used in order to investigate the best method of filling the ejection chamber with liquid. Finally a strobe system was integrated with the power supply circuitry such that the signal to the device that actuated the ejector triggered the strobe with an adjustable time delay (relative to the drive signal) allowing image capture of ejecting drop and piston motion sequences.

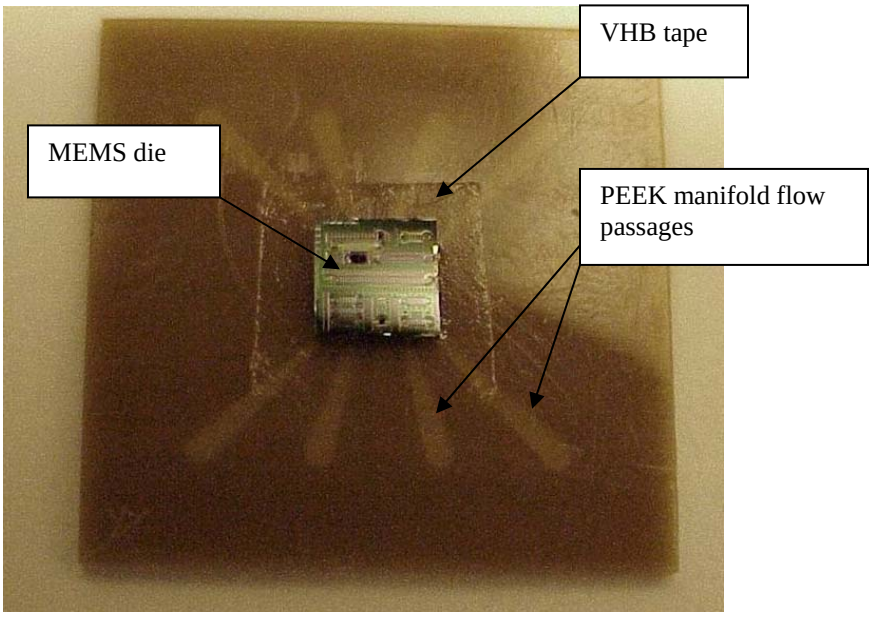

Figure 5a. Lowest package level – MEMS die to PEEK manifold

The first (smallest) level of MEMS ejector packaging is shown in Fig. 5a. The manifold that delivers liquid directly to the MEMS die is made from PEEK (Polyetheretherketone) a thermoplastic material with excellent inertness and dimensional stability. A flip-chip alignment machine (Finetech Picoplacer, Germany) is used to align the Bosch-etched fill holes in the back of the MEMS module to the exit holes of the PEEK flow manifold. Thin (0.001 inch) double sided tape (VHB tape from 3M, Minneapolis MN) with holes punched at the manifold exit hole locations holds the aligned die in place and seals the liquid connections at each hole. Passages in the PEEK manifold bring liquid to the MEMS fill holes from the next larger level of packaging – the acrylic flow control manifold shown in Fig. 5b.

The PEEK manifold inlet ports are sealed by mechanically clamping the PEEK part into the cut-out for the PEEK insert (Fig. 5b). Liquid is introduced into the control manifold through capillaries leading from pressure regulated reservoir fill bottles (Fig. 5c). Built-in needle valves allow flow to be controlled or cut-off to each of the PEEK flow passages (Fig. 5b). A built-in pressure transducer allows pressure to be measured both upstream and downstream of the MEMS device (Fig. 5b again). Eventually we intend to replace the manually adjusted needle valves with solenoid valves that will, in conjunction with the pressure transducers, allow automated feedback control of the pressure at the MEMS die.

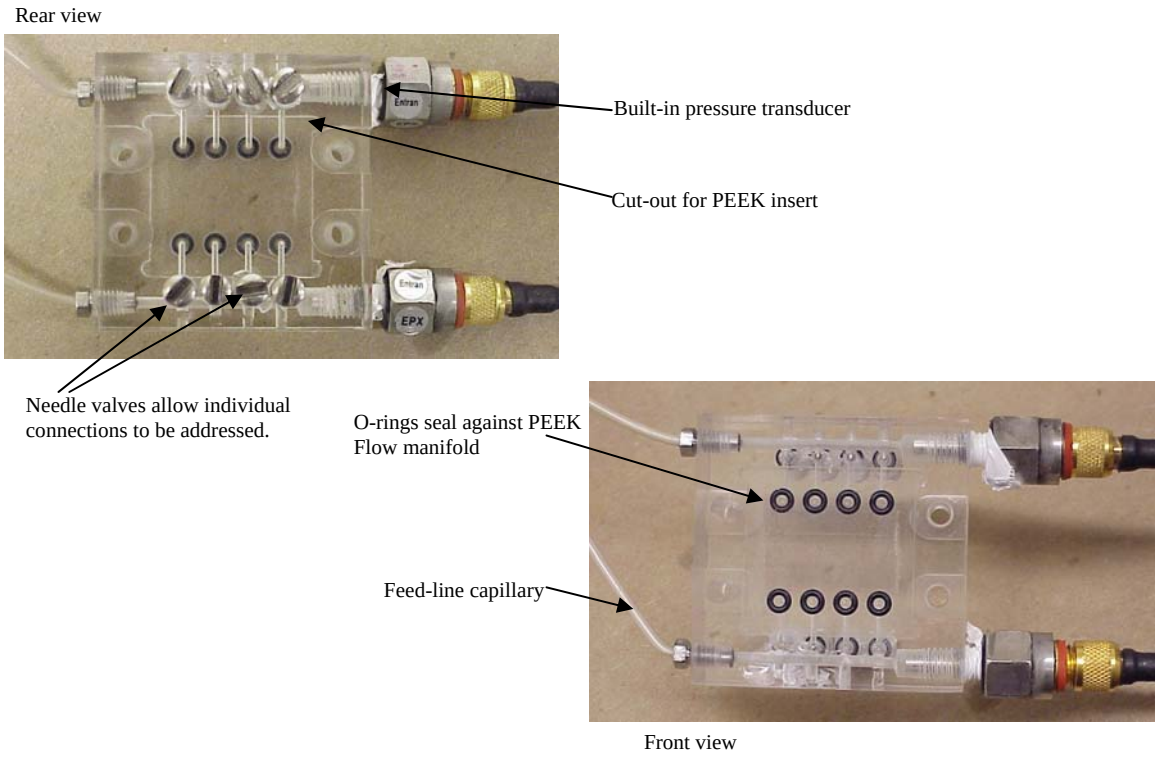

Figure 5b. 2nd level of packaging – acrylic control manifold for PEEK insert with mounted MEMS die.

The test station is shown in Fig. 5c. The packaged ejector, MEMS ejector die mounted on PEEK manifold, which is in turn mounted in the acrylic control manifold, is attached to support posts on a vibration isolated optical table such that drops are ejected horizontally. Optical access to the back of the transparent acrylic control manifold allows monitoring of the liquid meniscus into the MEMS die during filling. Two optical lens tubes provide magnified images both directed onto the nozzle plate (90 degrees) and at a 45 degree angle to the MEMS nozzle. The 45 degree angle view allows imaging of drop formation and ejection. The light pipe (Fig. 5c) direct the strobed light signal (1 μs pulses) onto the MEMS nozzle plate.

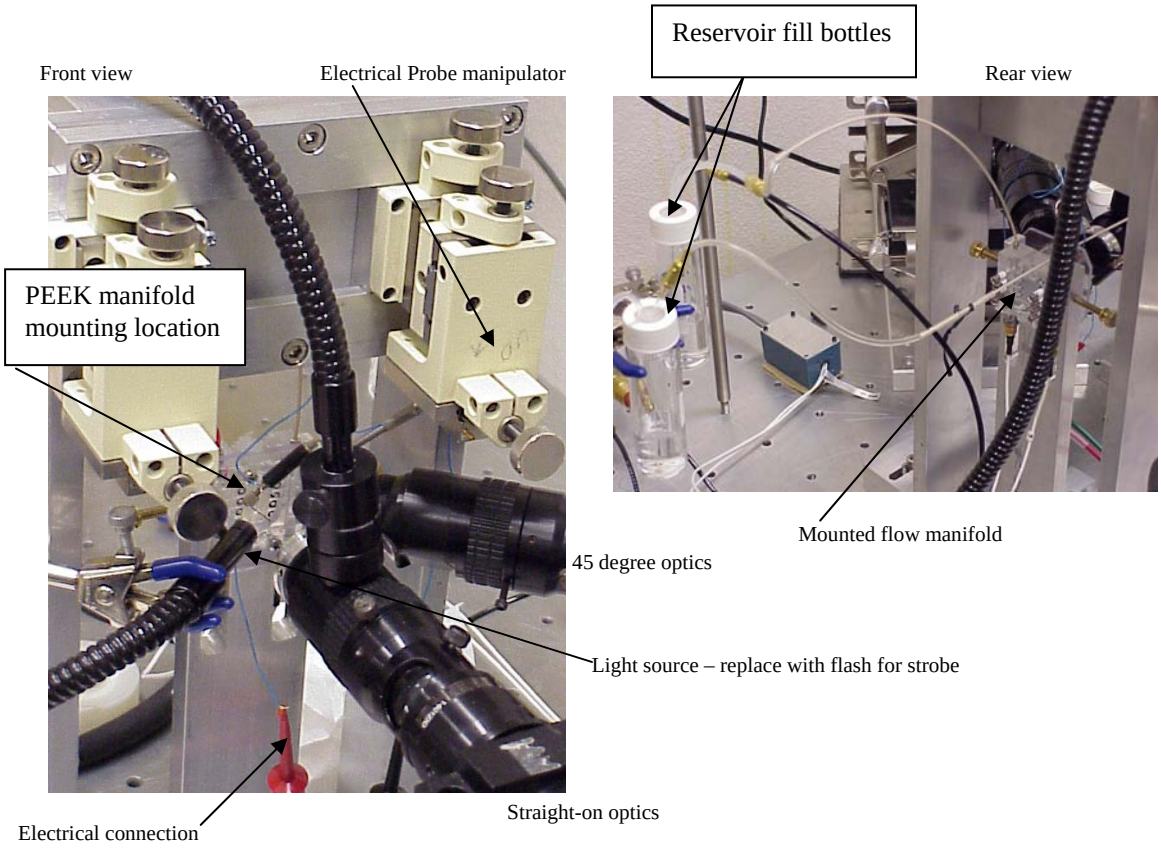

Figure 5c. Complete test station.

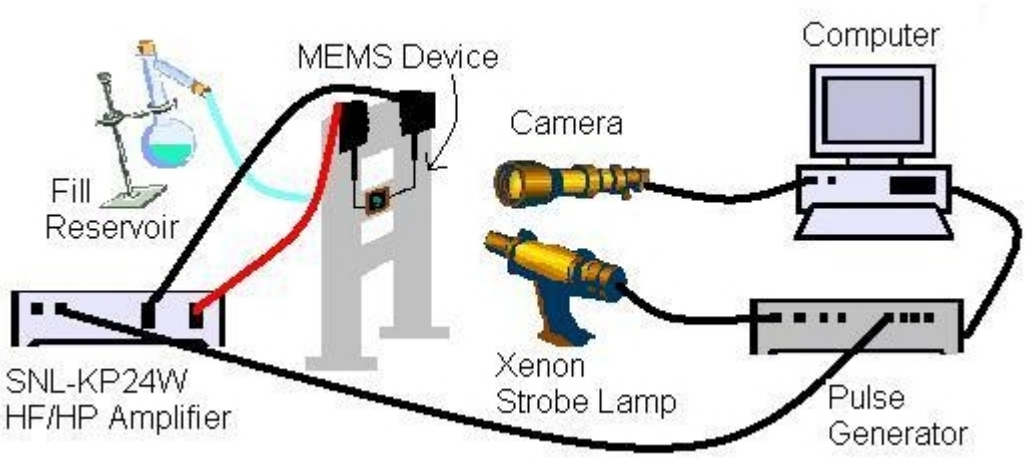

Figure 6. Test Station Schematic

Figure 6 shows a schematic of the test station experimental setup that measures the displacement of the MEMS sideshooter device and records the time-lapse video of the flight path of an ejected drop. The system is almost completely automated. The only manual component of operation is the application of a pressure head to the device, accomplished by adjusting the relative height of a water reservoir with respect to the device or via vacuum and pressure air lines at the bottle fill reservoirs. This could conceivably be automated through the use of pressure and vacuum valves that would be controlled through the computer program; however, it was not done in this experiment. The automated components of the measurement system are controlled through the use of MEMScript, a MEMS analysis software package developed here at Sandia National Laboratories. One MEMScript program allows control of the amplitude, length and frequency of the drive signal to the sideshooter. A GPIB signal is sent from the computer to a pulse generator that creates a waveform with typical amplitude, length and frequency of 2.8V, 10 μs, and 1 Hz, respectively. This pulse is sent through the amplifier which increases the amplitude to 75V without significantly altering the other aspects of the waveform. Simultaneously, the GPIB signal determines the timing and length of a TTL waveform that triggers the Xenon strobe flash. By varying the timing of the strobe flash trigger to occur at a time before, during, or after the actuation signal, an image can be captured that represents the state of the sideshooter, averaged over the length of the strobe flash. By looping through incremental delays of the strobe flash trigger, images can be captured that represent the state of the sideshooter at incremental times relative to the drive waveform. One image is generated at each successive piston actuation. The images are captured through a CCD camera by a separate program that is run concurrently with MEMScript. The images are stored in sequential order on the computer. Later, a different MEMScript program performs a pattern matching analysis on the images to calculate displacements of the sideshooter piston with respect to the drive waveform and drop ejection.

Aspects of the test station, especially the pressure control used to fill the MEMS ejection chamber, will eventually need to be incorporated into the complete patterning system during final test system integration. For now, the test setup allows us to evaluate the performance of the MEMS ejectors without having to perform the complete system integration.

MEMS Sideshooter Ejector Testing Results and Discussion

In order to eject drops the MEMS device must have the appropriate actuator and drive signal and be effectively filled with the liquid one plans to eject. The on-chip MEMS part of the microsystem integrates the filled chamber with the actuator in such a way as to still develop the required actuation force and piston velocity without a significant leak around the piston.

Actuator Characterization

The first step to testing any MEMS device is to determine if the MEMS actuator works as it was designed to. For these devices this involves applying an actuation voltage signal and measuring the motion of the MEMS piston using MEMSscript as described in the testing section just above. Initially a DC voltage actuation was applied to determine the voltage required for full piston travel and the spring constant of the actuator spring. This data provides a check on the analytically predicted spring constant and provides the minimum voltage level for actuator motion to a given displacement. The actuator will have to be actuated at a higher voltage and force to eject a drop in order to accelerate the drop. The signal that ejects the drop is expected to be on the order of 10 μs in rise time so a rapid rise time pulsed dry actuation is used to determine piston displacement at high speeds and the resulting maximum piston velocity that can be achieved. The DC and high speed dry test results will also provide data pertaining to the dynamic system analysis of the ejector (spring constant, damping coefficient, and inertia) that will allow ejector dynamics to be predicted in future devices. The dynamic system inertia and damping may be significantly effected by the presence of liquid in the device, which will modify the piston displacement relative to the dry actuation case.

Fig. 7a and 7b show typical results for the dry DC actuation of device 2 on the 2nd generation sideshooter module (RS424, module 8). All the devices behaved similarly during the DC actuation tests, although device 2 was the most reliable. Device 1, which ejected drops, was also quite reliable. The widest (300 μm wide piston) was not reliable and in many cases did not actuate under any voltage.

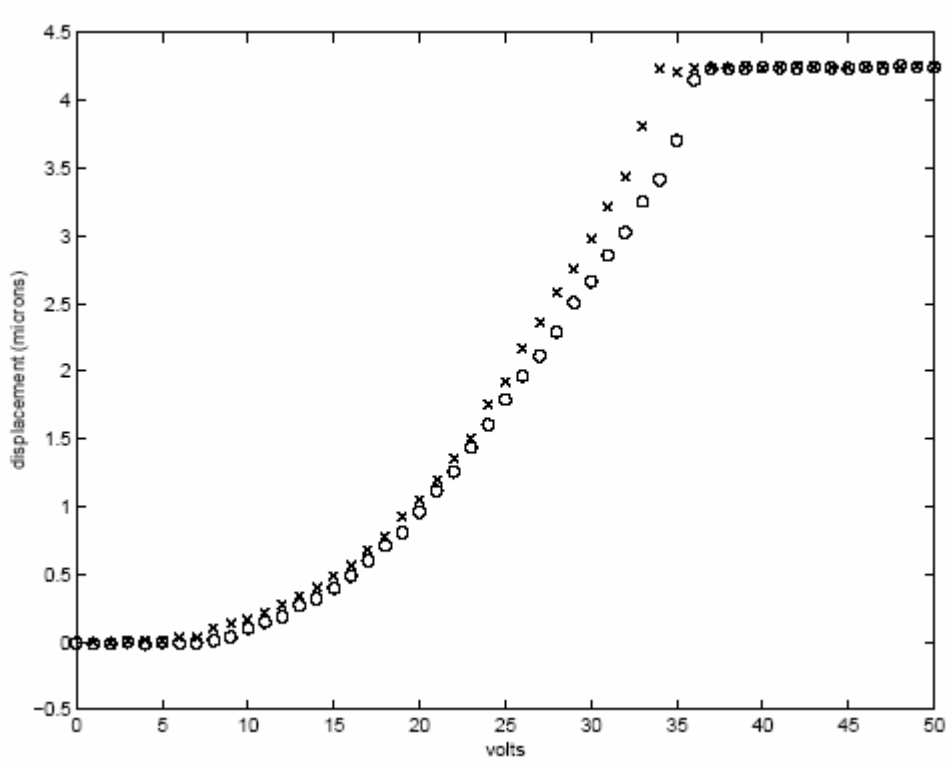

Figure 7a. DC Actuator Displacement as a Function of Voltage (RS424 module 8, device 2). Forward actuation (circles) and return actuation (x's).

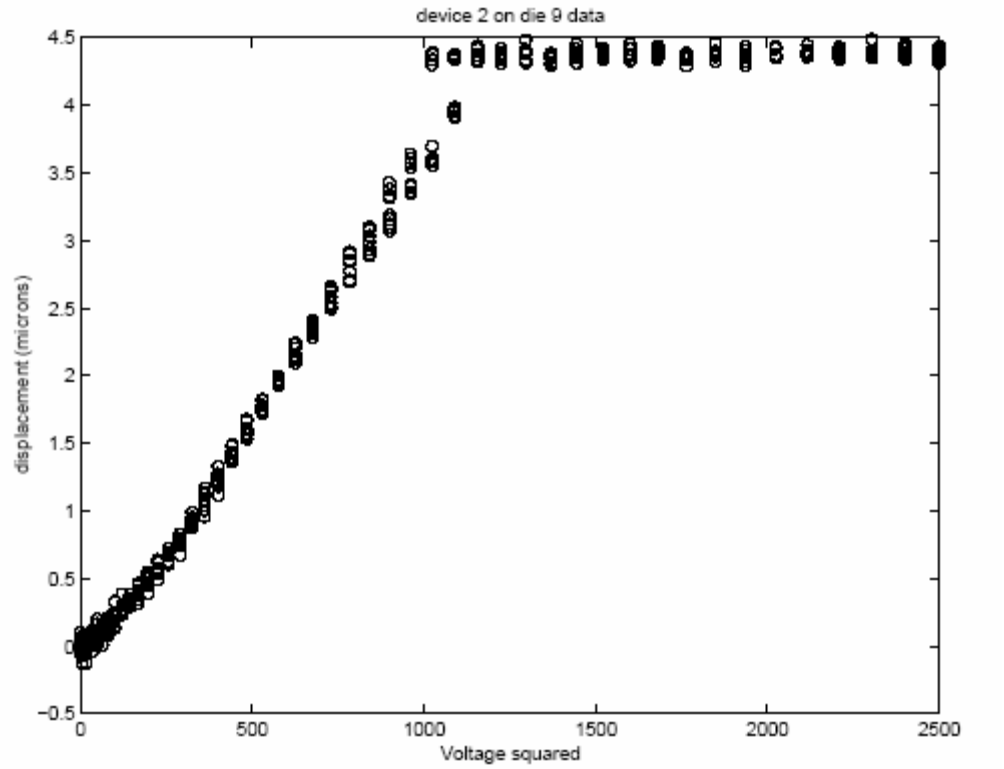

Figure 7b. V squared functionality of displacement.

Figure 7a shows the DC voltage required to achieve a given piston displacement. A hard stop at ~4.3 μm prevents deflection beyond this distance at higher actuation voltages. The difference between forward and return actuation (voltage ramped up to 50V then back down to 0V in 1V increments) is probably due to stiction. Stiction is 'sticky friction', a MEMS frictional effect that is indicated by moving parts being stuck down to the substrate or a stationary MEMS structure until enough force is applied to break them free. Approximately 7V is required to break the piston free from is 0V position, corresponding to a start-up force of ~0.5 μN (from Eqn. 1). Similarly hysterisis is evident is evident during the return stroke. Stiction between the actuator stop and the moving piston structure results in a net return force of ~0.15 μN (again Eqn. 1) required to break the actuator loose and begin the return stroke. Figure 7b. shows the voltage squared functionality of displacement, as predicted from Eqn. 1. By fitting a straight line to the linear part of the curve (between approximately 500 and 1000 V^2) the spring constant for these actuators can be calculated. This calculation yields a spring constant of k = 50 μN/μm.

Figure 8 shows the effect of actuation voltage suddenly applied (high speed actuation – signal rise time on the order of 3 μs, 0% to 100% of actuation voltage) for device 1 RS424 (drop ejecting design). The higher voltage is able to accelerate the piston faster to its full travel. For all three voltages plotted the piston position appears to bounce at approximately 4 μm (slightly before the actuator hard stop) and then vibrate as it finishes reaching the full extent of its travel. The voltage is applied for a relatively long time (~100 μs or even longer) for all three voltages. The faster displacement at the higher voltages results in the displacements being out of phase as they vibrate. The 2nd part of Fig. 8 is identical to the first part but the time scale is shorter to allow us to focus in on the high velocity portion of the curve. Straight line curve fit slopes of position vs time during the period of maximum piston velocity yield piston velocities of U_p = 0.615 μm/μs at 40V actuation, 0.958 μm/μs at 50V actuation, and 1.04 μm/μs at 60V actuation. Since we estimate that ~1 μm/μs will lead to drop ejection a signal greater than 60V will probably be required for drop ejection.

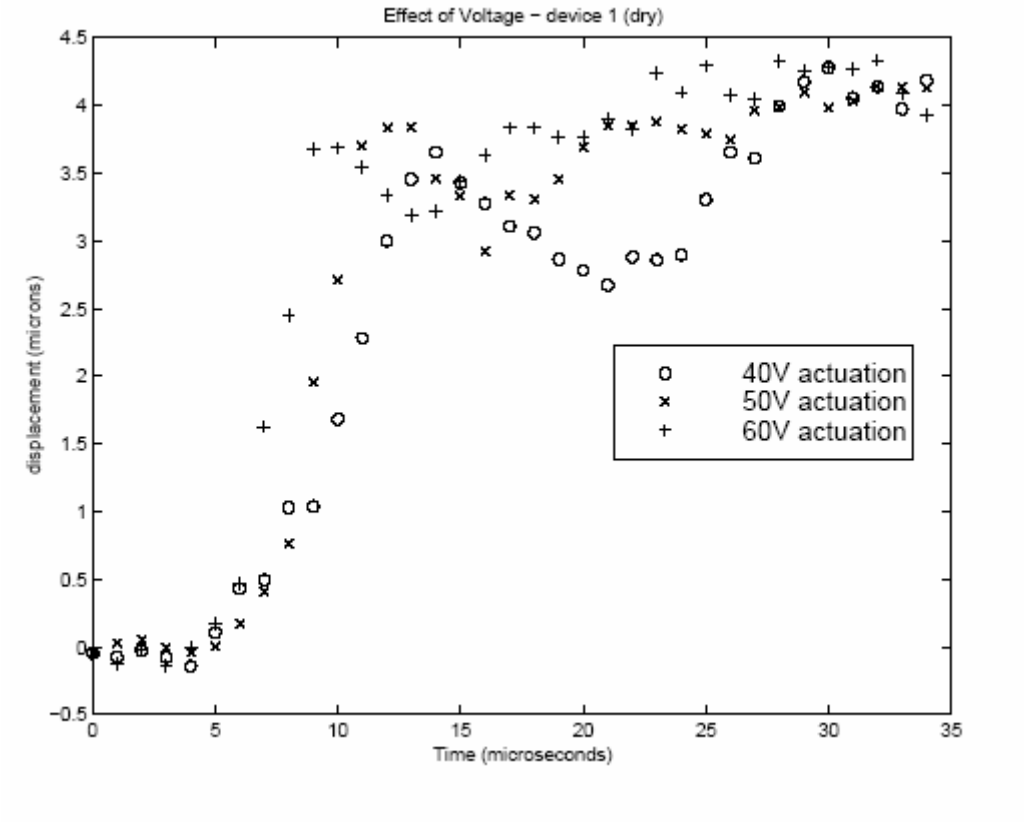

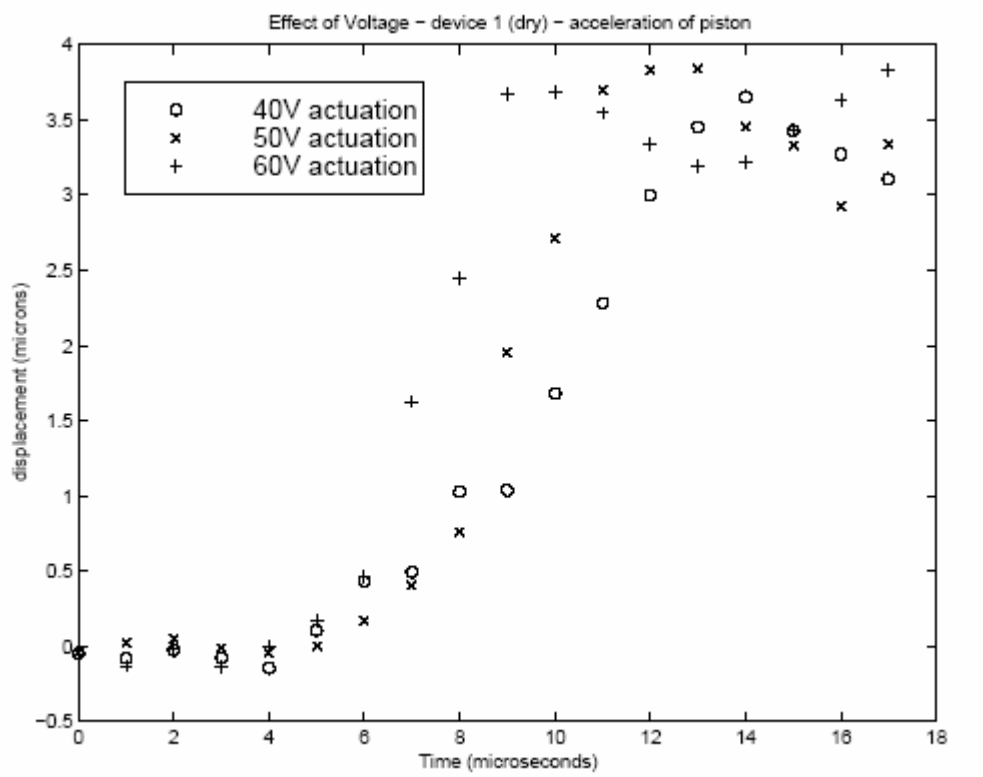

Figure 8. Effect of voltage at high frequency actuation (35 and 18 microsecond time scales).

Additional vibrating or ringing phenomena were observed when the effect of pulse width on piston actuation displacement was investigated (Fig. 9). The pulse width investigation revealed the minimum time for signal application that is required for full actuator travel. The 10 μs pulse width signal application was not long enough to achieve full displacement while the 50 μs signal application was (Fig. 9). There is a delay from the time the signal is first applied until the actuator begins to move of about 5 μs, during which the voltage pulse is reaching its maximum value (~3μs) and actuator stiction is overcome. Then there is a period of rapid acceleration from about 4 to 8 μs after pulse initiation, followed by a period of approximately constant maximum velocity travel until about 12 μs after pulse initiation. The actuator appears to bounce before it hits the stop and then complete its full travel by approximately 15 to 20 μs. Since the full time of high velocity piston travel is needed in order to eject a drop (Fig. 19) a signal pulse width of at least 12-15 μs is required for drop ejection. Summarizing the results of the dry pulse width and voltage effect investigations; in order to achieve full displacement, high velocity actuator travel needed for drop ejection, a voltage signal of at least 60V for 12 μs is required. The presence of liquid in the ejector will increase the voltage required to achieve the high piston velocity for drop ejection.

The second interesting effect observed during the pulse width investigation is the natural vibration response of the ejector actuator at the end of the signal pulse when the voltage suddenly drops to 0V. The ring-down in displacement amplitude (Fig. 9) shows an under-damped system response. The period of oscillation is about 20 μs, corresponding to a natural frequency of ω_n = 1/20 x 10^{-6} = 50,000 rad/s ($f_n = \omega_n / 2\pi$ = 7958 Hz – approximately 8 kHz). This natural frequency measurement allows determination of an effective system inertia (mass), since we have already determined system stiffness.

$$\omega_n = \sqrt{\frac{k}{m}} = 50{,}000 \quad m = \frac{k}{\omega_n^2} = \frac{50}{50{,}000^2} = 2\times10^{-8}\ kg$$

The damping coefficient can also be estimated from the data shown in Fig. 9. The 10 μs data contains several cycles from which the exponential decay factor can be determined. The amplitude envelope for the decaying oscillating under-damped response (Fig. 9 – 10 μs data) is reduced to 1/e = 0.3679 of its starting amplitude of ~3 μm in approximately τ = 50 μs. The complicating effect of the actuator back-stop that prevents full amplitude oscillation in the negative direction (-1 μm displacement limit in Fig. 9) is ignored in this simplified calculation. The damping coefficient can be calculated from the characteristic decay time (τ).

$$c = \frac{2m}{\tau} = \frac{2 \cdot 2 \times 10^{-8}}{50 \times 10^{-6}} = 8 \times 10^{-4} \ N - s / m$$

The high speed dry piston motion analysis has revealed the coefficients needed to understand the actuator motion (actuator mass, stiffness, and damping coefficient). These coefficients will be modified when liquid is filled into the ejection chamber. Specifically the damping coefficient and the inertia of the actuator should vary. The effect of the liquid on the inertia can be estimated by calculating the mass of the liquid in the ejection chamber, which will be pushed by the piston and in effect add to the mass of the piston. The ejection chamber volume is approximately 50 μm x 50 μm x 10 μm = 2.5 x 10^{-14} m^3. When filled with water (ρ = 10^3 kg/m^3) this volume has a mass of 2.5 x 10^{-11} kg. This mass is 4 orders of magnitude less than the dry system inertia, therefore the presence of liquid should not significantly slow down piston actuation velocity due to inertia effects.

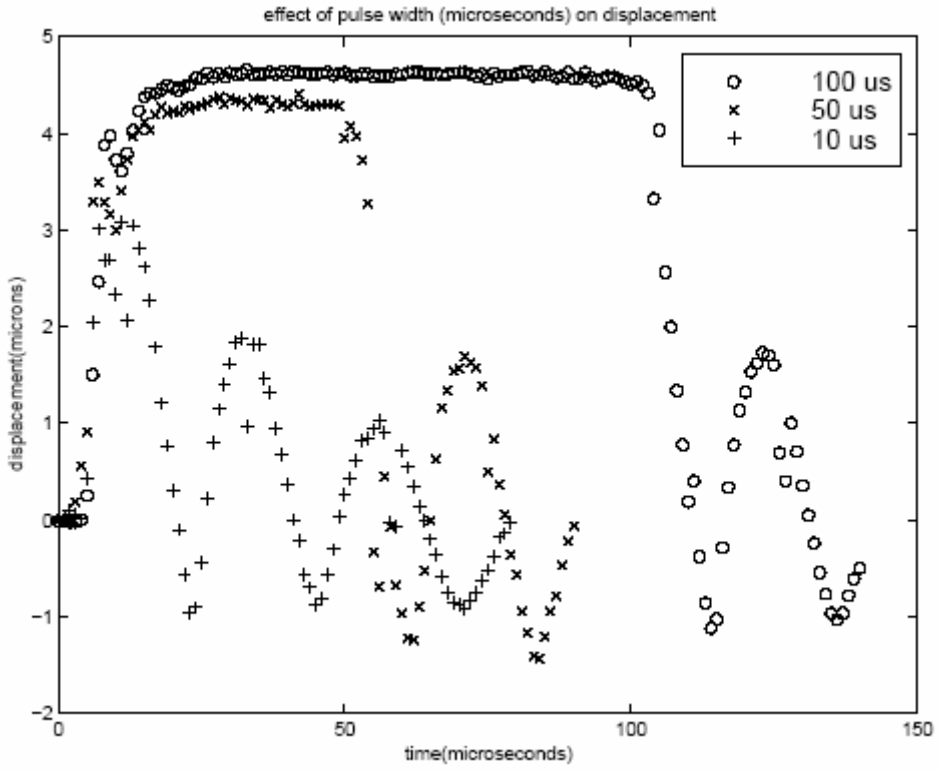

Figure 9. Effect of pulse width – high frequency actuation at 65V – device 2 RS424 module 8.

Ejection Chamber Liquid Filling

The way in which the ejection chamber fills with water (or other liquids for that matter) depends on the wetting characteristics of the polysilicon surfaces. As described earlier there are two different surface finishes that result from our drying processes – a hydrophilic surface (SCCO2 drying) and a hydrophobic surface (VSAM). These two finishes caused different chamber filling characteristics. One would think that the hydrophilic finish would be easier to fill as water would almost spontaneously wick into the device, however in practice this process proved to be difficult to control and water leaked out around the piston very easily in the hydrophilic case. This can be understood when one considers that a small positive pressure is generally required to fill the flow manifold up to the MEMS ejector (a vacuum pulls air into the manifold through the ejector – the opposite of filling with liquid) and the hydrophilic surface produces a local vacuum to draw liquid in as soon as it starts to wet. This is an unstable pressure configuration and the pressure difference between the upstream filling manifold pressure and the in-device wicking pressure suddenly increases upon MEMS surface wetting, leading to more rapid filling and even a larger pressure difference. A future design for these ejector chambers should incorporate a more clever filling geometry that will spontaneously fill the ejection chamber but not leak when the surface is hydrophilic.

The filling processes could be observed by following the meniscus as it entered the ejection chamber. A special fabrication run utilized a transparent silicon nitride ejection chamber cover that allowed us to see and capture images of meniscus motion during filling. The hydrophilic meniscus images are shown in Figs. 10 – 12. The images in Figures 10 and 11 show typical filling patterns that occurred at low pressure (0.3 psi). The hydrophilic meniscus angle is clearly shown in Fig. 10 on the fill passage sidewalls. The angle is approximately 35 degrees. Figure 10 also shows that the devices were typically partially filled. A trapped air bubble in the ejection chamber inhibits complete filling. In these silicon nitride cover devices the ejector nozzle was not fabricated. The nozzle would provide an escape path for this trapped air, so the devices with the nozzles should fill more readily. Even with the nozzle, however, we had trouble filling the hydrophilic devices. After partial filling, pressure was increased in an attempt to force out trapped air bubbles. Generally there was no change in meniscus pattern until a threshold pressure was attained and the device filled and liquid leaked out around the nozzle shaft and flooded the ejector (Fig. 11). The right hand image in figure 11 shows less extensive flooding than the right hand image because the blocking wall/wick (see Fig. 4) has effectively routed the liquid away from the comb drives. In the left hand image there was too much liquid wicking onto the front surface and the blocking wall/wick was unable to reroute the flow, flooding has inundated the comb drive and it is inoperable. Upon leaking out around the piston, liquid wicks all the way around the outside edge of the ejection chamber housing (Fig 11) because the corner of the housing/substrate interface, is a low surface energy location that is highly favorable to wetting.

Figure 12 shows a successful (one of the few) filling sequence of the hydrophilic ejection chamber (device 17 on RS349 – 1st generation ejectors with the transparent silicon nitride cover). Initially water wicks into and partially fills the passage (0 and 0.1 psi). The hydrophilic meniscus shape and contact angle is clearly visible. The bubble seal does not wet and is providing a barrier to leaks around the piston shaft. As the pressure is increased, liquid wicks around the edge of the ejection chamber, leaving an air bubble in the center of the chamber (0.11 and 0.25 psi). A centered ejector nozzle would be easier to completely fill without trapped bubbles than one with the nozzle at an edge of the chamber because of this effect. At 0.25 psi the ejection bubble seals appear to fill with liquid, and at 0.3 psi liquid appears to completely fill the ejection chamber, perhaps with the air bubble still trapped in the ejection chamber but now surrounded on all sides by liquid.

Much more success was achieved with the hydrophobic finish. Higher pressures were required to fill the devices and we were better able to control these pressures as a gradually increasing pressure was required to fill the ejection chamber. The devices that successfully ejected drops were hydrophobically treated (VSAM) and once we established the procedure for filling these devices, they filled reliably. Hydrophobic ((VSAM) filling is shown in Figs. 13-15. Figure 13 shows the typical hydrophobic meniscus shape with a contact angle > 90 degrees (~110 degrees) as water is forced into the chamber at a pressure of 1.5 psi. Notice that the hydrophobic data shows higher pressures (generally at least 1 psi higher) required to fill hydrophobic devices as compared to hydrophilic devices.

Figure 14 shows a sequence of meniscus motion during filling of hydrophobically released device 17 (same device as is shown filling for the hydrophilic case in Fig. 12). The inlet passage gradually fills with liquid as pressure is increased from 1.5 to 2.6 psi. Fig. 15 shows a successful filling sequence with a transparent silicon nitride cover that allows us to track the meniscus during a complete fill. At 0.82 psi the meniscus is seen just breaking into the ejection chamber from the inlet passage. At 0.86 psi water has completely filled the ejection chamber and the meniscus is no longer visible in the chamber. The meniscus can be seen at about half way along the piston pinned at the end of one of the guide dimples. At 0.96 psi the chamber is still filled, no leaks have developed and the meniscus is barely visible pinned at the point where the piston shaft leaves the ejection chamber housing by the bubble seal. The meniscus motion is much easier to see in a video format.

Images in Figs 16 and 17 show successful filling of device 1 on RS424 – a design that successfully ejected drops. This device was hydrophobic (VSAM). Both the straight-on and 45 degree views are shown in these figures. Upon filling this device leaked slightly out of the ejector nozzle but did not leak around the piston at all (Fig. 17). By dropping the pressure back to atmospheric we were able to pull the leaked droplet back into the chamber prior to initiating ejection actuation.

Once the ejection chambers were completely filled we were ready to try applying the actuation signal to eject a drop. If the devices were effectively filled without leaks, in general, no leaks developed during the actuation stroke. Liquid was pulled along with the piston even as is tried to flow around the moving piston and the net position of the meniscus around the piston remained approximately the same. Once the device was correctly filled it did not leak.

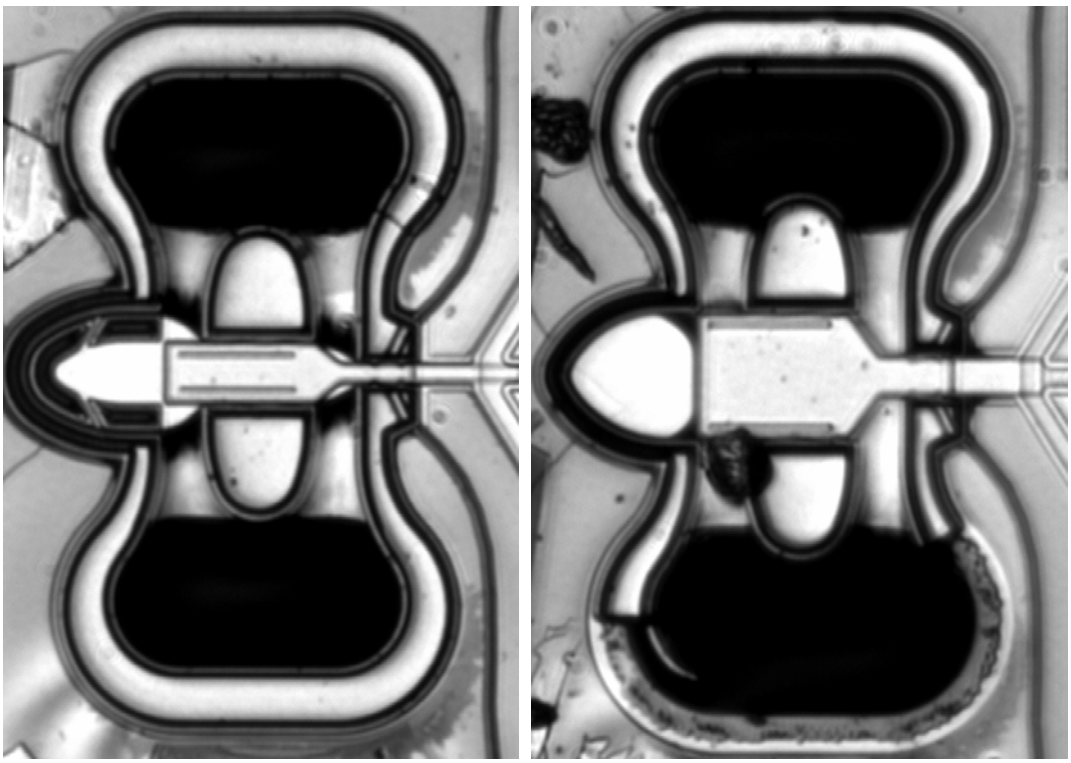

device 12 – 0.3 psi device13 0.3 psi

Figure 10. Hydrophilic filling – wick-in.

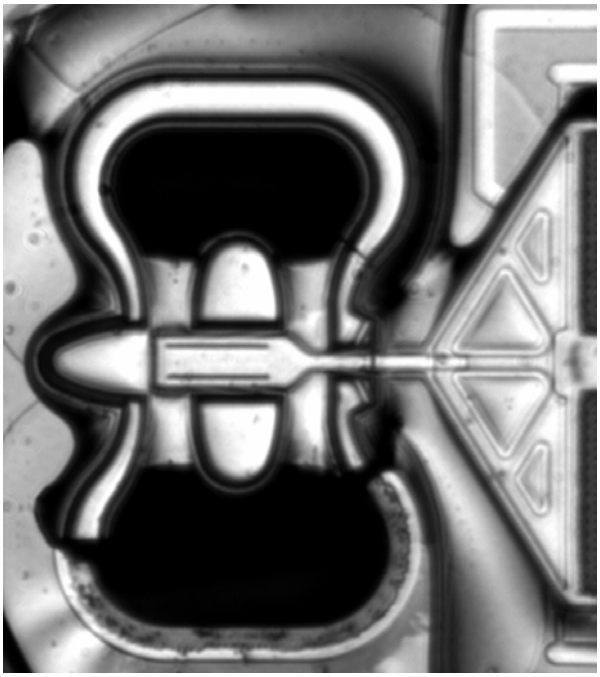

device 7 flood 0.3 psi

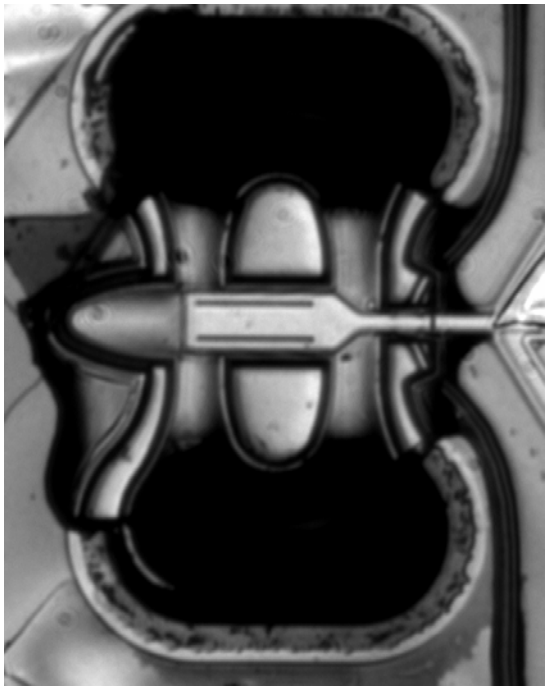

Device 8 at 0.34 psi

Figure 11. Hydrophilic filling – flood.

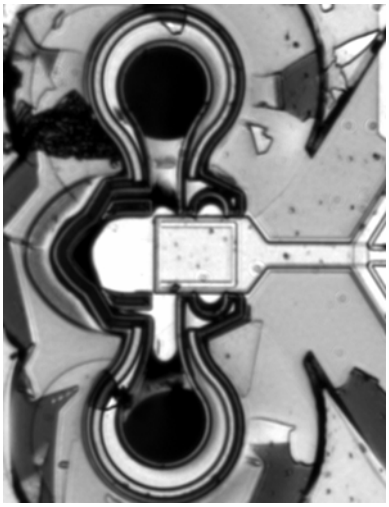

Device 17 fill – 0 psi

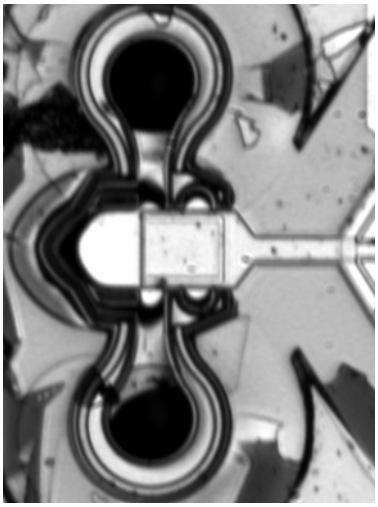

Device 17 – 0.1 psi

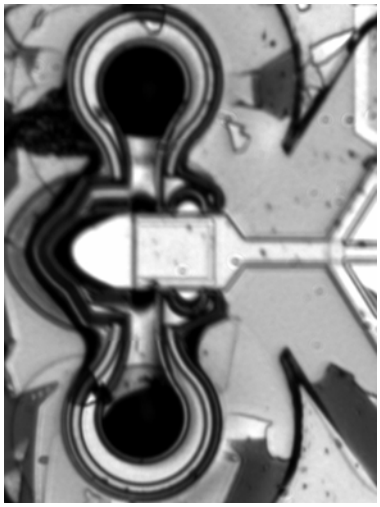

Device 17 0.11 psi

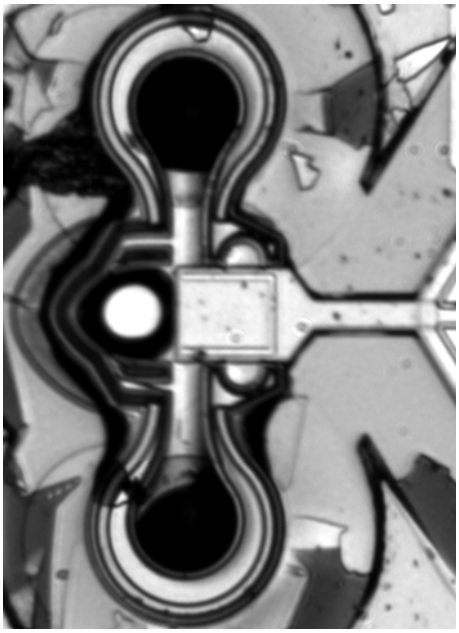

Device 17 – 0.25 psi

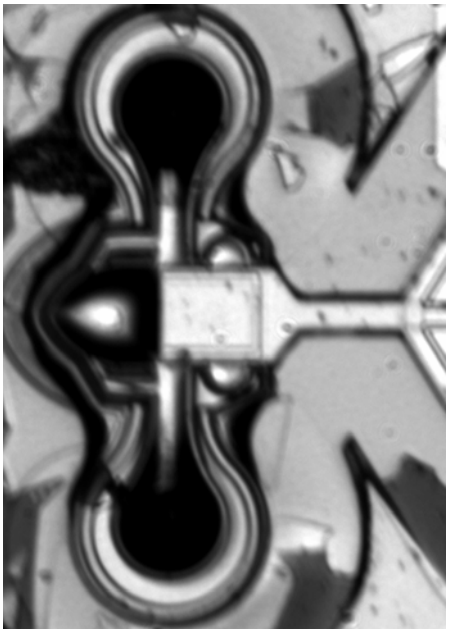

Device 17 0.3 psi

Figure 12. Hydrophilic fill sequence – Device 17.

dev 13 1.5 psi

Figure 13. Hydrophobic filling meniscus shape.

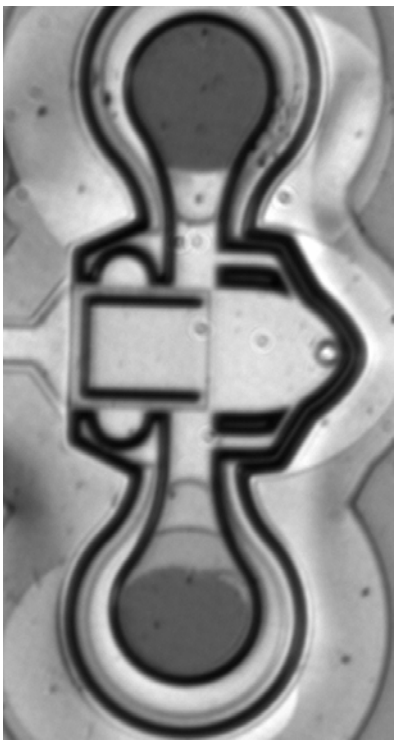

dev 17 1.5 psi

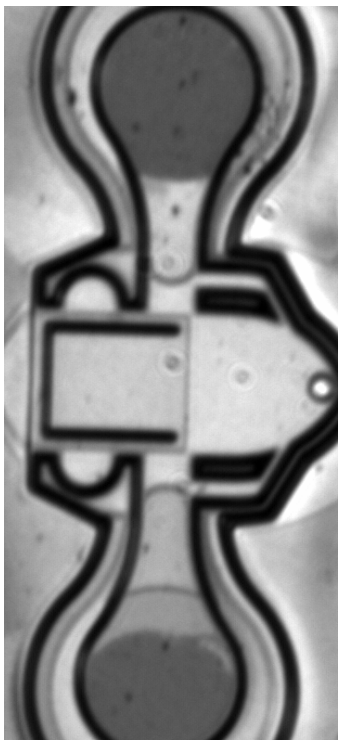

device 17 1.75 psi

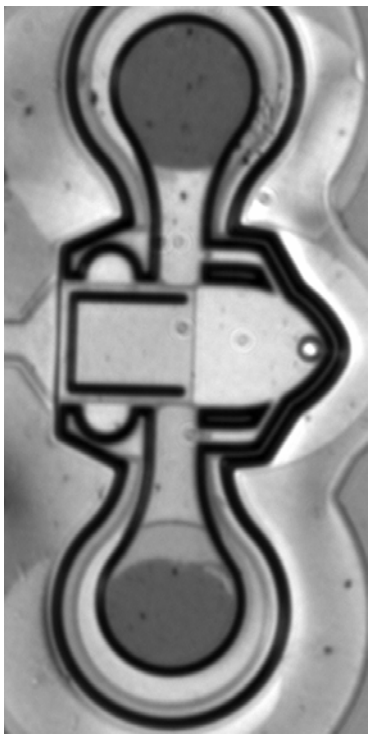

device 17 – 2.6 psi

Figure 14. Hydrophobic filling sequence – device 17.

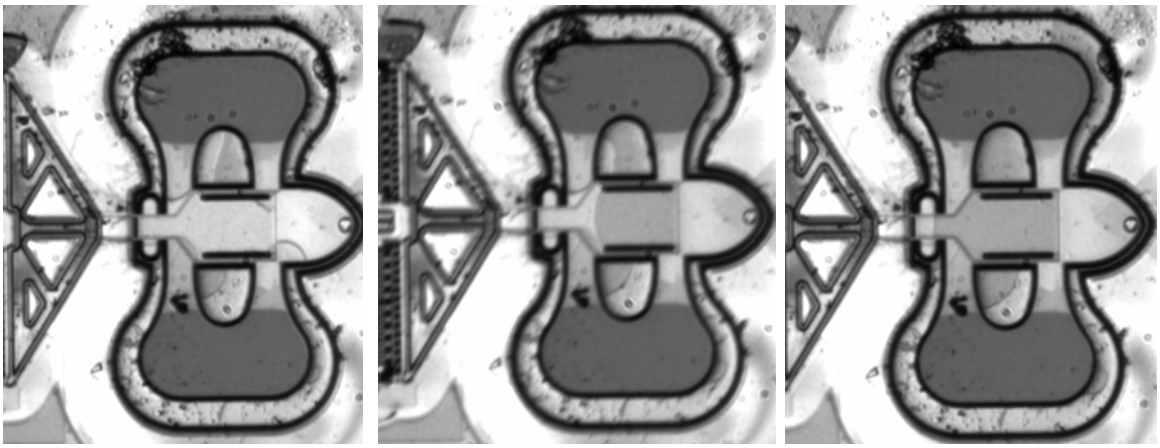

menisci-fill 0.82 psi menisci-fill 0.86a psi menis-fill 0.96a psi

Figure 15. Hydrophobic filling sequence – successful filling.

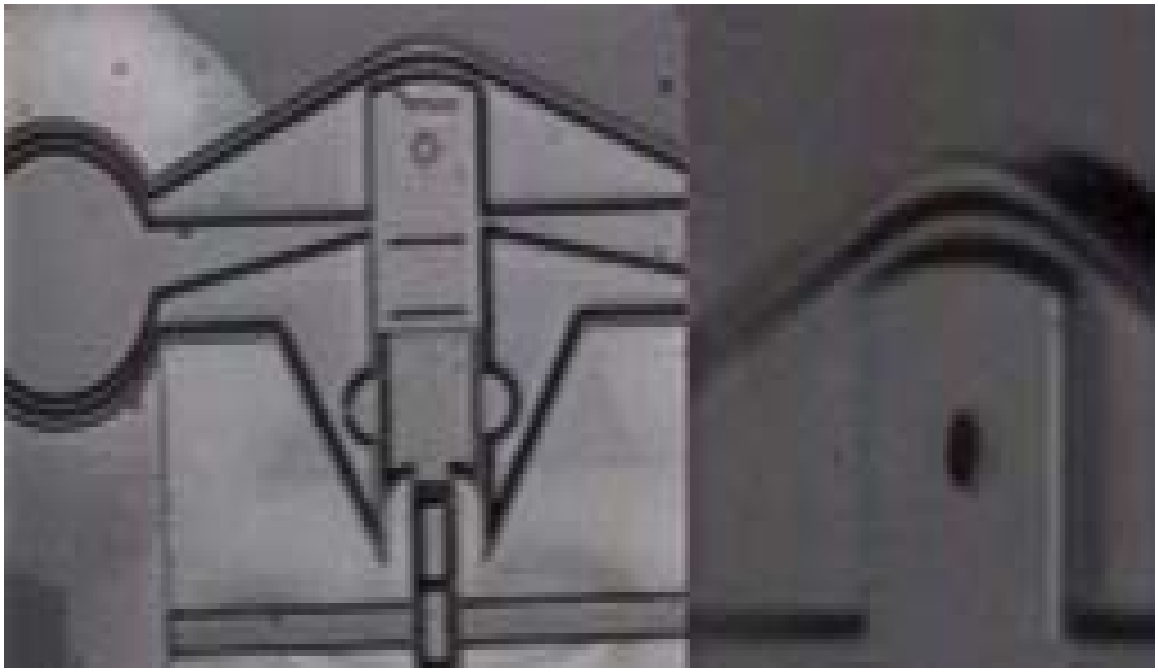

Figure 16. successful fill device 1 RS424 – pressure just before fill 0.5 psi

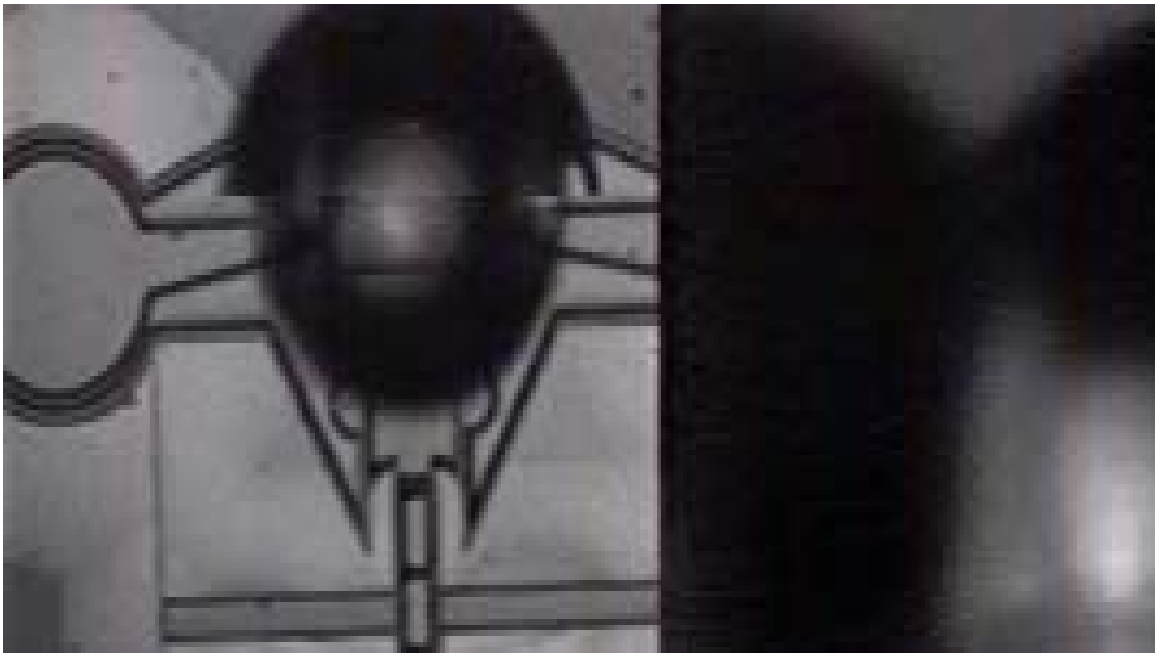

Figure 17. successful fill of dev 1 RS424 – just after fill – 0.61 psi.

Drop Ejection – wet actuation

The application of a 1 Hz, 80V, 12 to 20 μs pulse signal with a fast rise time (~3 μs) to the 21 bank HPCD actuator resulted in water drop ejection from device 1 on RS424. Lower voltages or faster pulses did not produce drops. Longer pulses did produce drops. Attempts to apply larger voltage to the actuator generally resulted in actuator failure. This actuator is in the edge of operation at 80V. To reduce the voltage required a design with more than 21 actuator banks is needed. Drop ejection was performed repeatedly for this design from several different modules and from a similar design with the longer actuator stroke length (device 14 on RS424), indicating a degree of reliability with this drop ejection concept which was not evident with the 'roofshooter' concept referred to earlier [9]. At higher actuation frequencies (1 kHz instead of 1 Hz) the sideshooter was less reliable.

Stobed images at 2 μs increments of drop ejection are shown in Fig. 18. The nozzle showed no drop meniscus forming until about 8 μs after signal application. This time corresponds to the high velocity portion of the piston actuator motion (shown in Fig. 19). A drop then rapidly emerges from the ejector nozzle and is completely formed by 12 μs. At 12 μs the actuation signal goes to zero and the piston springs back toward its original position. This corresponds to drop break-off at 14 μs (see Fig. 18). The drop break-off is clean and does not involve the breakup of a long liquid jet into satellite droplets. This sideshooter inherently ejects single drops without satellites because of the mechanism of drop ejection and the sudden retraction of the piston. The ringing phenomena observed during dry actuation was not observed during drop ejection – indicating that the liquid has significantly damped the actuator motion and the system is now over damped (see Fig. 19). The higher voltage (and force) required for wet high velocity actuation (80V – 1.25 mN, wet as opposed to 65V – 1 mN dry) is needed to overcome the damping and develop the high piston and corresponding drop velocities needed for ejection.

The velocity of the ejected drop can be estimated from measuring the distance that the drop has moved in strobed image frames separated by a known time (Fig. 18), and the piston velocity can be determined from the displacement data (Fig. 19). The piston velocity is estimated at 1-2 m/s (1-2 μm/μs) from Fig. 19

during drop ejection (5-10 μs after the initiation of the actuation signal), and the drop velocity was determined to be 5-10 m/s (5-10 μm/μs) just after drop break-off (Fig 18 after break-off frames).

The drop diameter can be estimated by comparing it to the known diameter of the ejector nozzle (10 μm for this ejector design) in the images shown in Fig. 18. The diameter determined from this method is slightly smaller than the nozzle diameter (8 μm). This corresponds to a spherical drop volume of approximately 0.25 picoliters of water.

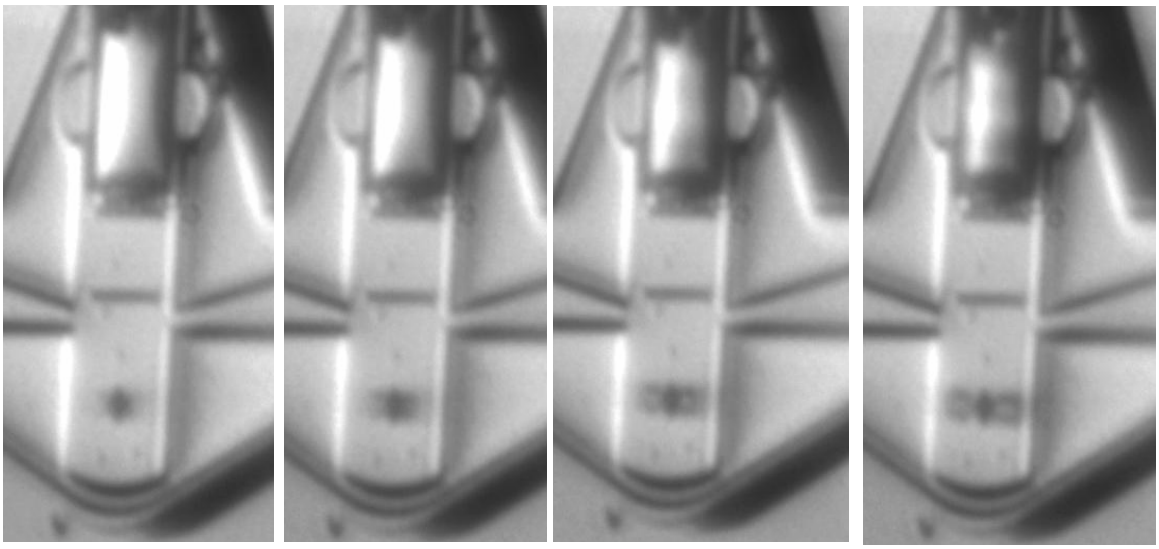

6 μs. 8 μs. 10 μs 12 μs

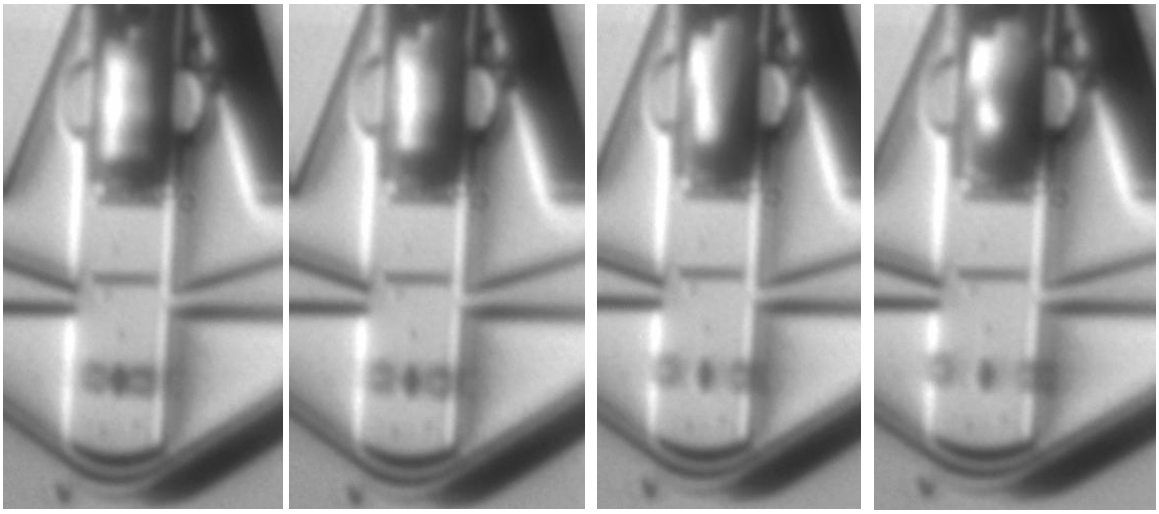

12 μs 14 μs 16 μs 18 μs

Figure 18. Stoboscopic images of drop ejection – device 1, RS424 module 8 with 80V actuation for 12 μs.

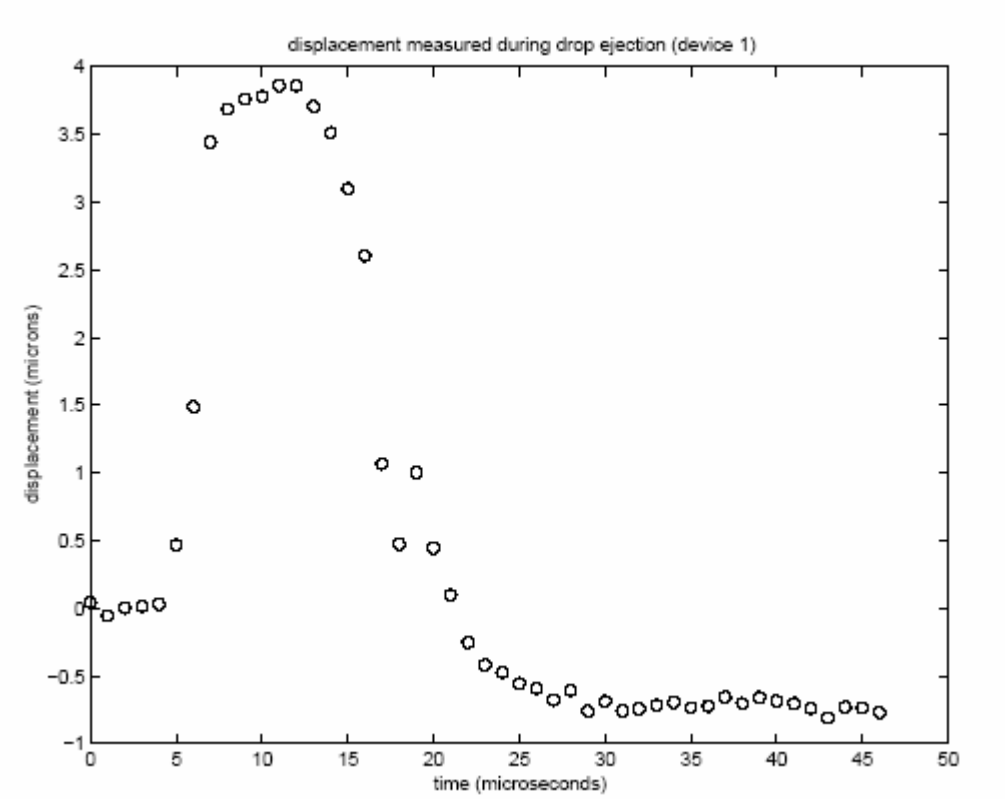

Figure 19. piston motion during ejection (images just above)

Electro-Microfluidic Packaging for Sideshooter Drop Ejector

Introduction:

The desire to incorporate electrical and fluidic connections on-chip has lead to the development of a novel packaging architecture [15] that has found an application in this MEMS ejector manufacturing system. This unique approach effectively integrates macro-scale electrical and fluidic connections with similar micro-scale features required for current MEMS electro-microfluidic devices. The multi-level package design features a Fluidic Printed Wiring Board (FPWB) designed to interface with an Electro-Microfluidic Dual In-Line package (EMDIP™). The EMDIP represents the first level package and is designed to accommodate a wide variety of electro-microfluidic devices. The EMDIP contains a meso-scale, fan-out manifold that, on one side, mates directly with small (down to 50 micron diameter Bosch™ etched holes) found on the back side of the MEMS device, and, on the other side, mates to larger 1mm diameter holes located in the EMDIP base. Machined channels in the meso-manifold efficiently transfer fluid from macroscopic volumes (microliters or milliliters) down to microscopic volumes (picoliters). The second level package, the FPWB, acts as the foundation for the first level package and provides links to the electrical and fluidic connections found on the first level package. In addition, the FPWB contains the macro-scale electrical and fluidic connections that connect to larger, third level, systems.

While it is often difficult to produce components with features of such small magnitude, each level in the packaging architecture can be easily manufactured using traditional machining processes such as mill, CNC and wire EDM. Non-traditional machining processes such as stereolithography and selective laser sintering may also be used. A variety of materials including thermoplastics, thermosets, glass and ceramics can be used in the manufacture of each packaging component; however, fluid compatibility, cost and availability generally define material selection. In order to minimize the number of different materials that the fluid contacts, it is desirable to fabricate the first and second level packages out of the same material. Also, identical materials for both the first level and second level will negate any concerns regarding mismatch of the thermal coefficient of expansion. A high temperature thermoplastic, Polyetheretherketone (PEEK™) was chosen for this package based on its exceptional fluid compatibility characteristics.

Overview of electro-microfluidic package:

The Fluidic Printed Wiring Board (FPWB) represents the second level in the packaging architecture and serves as the foundation for the entire electro-microfluidic package design. Figure 20 shows an exploded view of the FPWB, electrical connector, and fluidic connector. The design and manufacture of the FPWB is similar to a general Printed Wiring Board (PWB); however, there is one key difference. The material used to manufacture the FPWB would typically not be standard PWB material (e.g. FR4 or Thermount). As stated above, the material chosen for the FPWB is PEEK™, a chemically inert, high temperature thermoplastic. In general, the FPWB consists of two parts, the channel board and the cover board. The channel board would typically be thicker than the cover board to accommodate the channel depth and threaded flat-bottom ports located along the edge. The current channel board thickness is 5mm. The six individual channels in the channel board are machined to eliminate sharp edges to prevent stagnant fluid build up. The six flat-bottom threaded ports located in the side of the channel board interface with standard #6-40 fluidic connectors. The cover board fits on top of the channel board and contains six through holes that align with the machined channels in the channel board. The cover board also contains the electrical traces that connect a standard 24-pin ribbon connector to the wire bond pads located in the center of the board. The FPWB is assembled by attaching these two boards together.

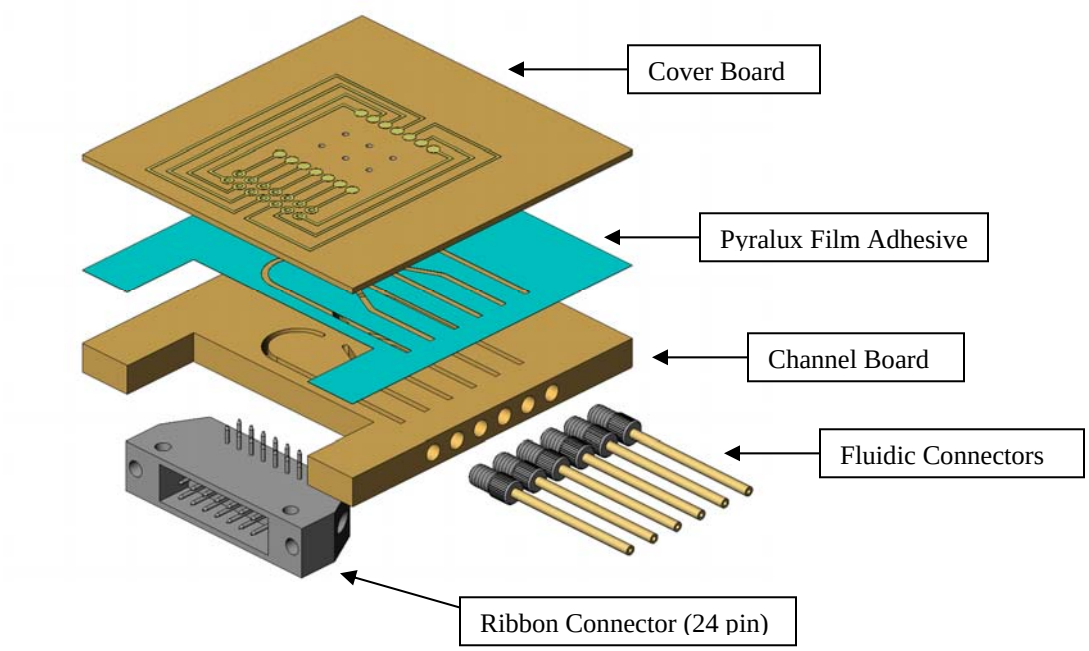

Figure 20: Exploded view of Fluidic Printed Wiring Board (FPWB) with a standard 24 pin electrical connector and six #6-40 Upchurch Scientific fluidic connectors.

The electro-microfluidic package design consists of two levels. The FPWB is the second level package and is designed to interface with standard electronic and fluidic components as well as multiple EMDIP™. The EMDIP™ was developed as a first level package for electro-microfluidic devices. This packaging methodology is analogous to the Dual-In-Line Package often used to package Integrated Circuits (ICs). Figure 21 shows an exploded view of the 24-pin, 8 channel EMDIP™. This particular configuration allows for connecting the electro-microfluidic device to a maximum of 24 independent electrical connections and 8 individual fluidic connections. The EMDIP™ is constructed in layers. The base looks like a modified DIP (Dual In-line Package). The spacing for the electrical leads is standard and will plug into a standard DIP socket. The base contains eight 1mm through holes that become the fluidic interfaces to the second level package. Along the periphery of the cavity in the base are the bond pads that are available for wire bonding to the bond pads found on the top surface of the electro-microfluidic device. A meso-scale, fan-out manifold is contained within the cavity of the base and contains six tapered fluidic channels that provide a gradual transition from the 1mm diameter holes found on the base to the 50 micron bosch™ etched holes found on the electro-microfluidic device. The tapered channel design eliminates sharp corners in the channel and reduces locations that stagnant fluid can collect. An adhesive tape is used to secure the manifold to the base. To reduce risk of fluid contamination, the adhesive tape can be applied to the manifold before the channels are machined to produce the same channel footprint in the tape. Similarly, the adhesive tape is used to attach the electro-microfluidic device to the manifold. The adhesive tape may also be applied to the backside of the manifold before machining to produce the same through hole footprint. Please note, while EMDIP™ can be used to package a variety of electro-microfluidic devices it was not used to package the Sideshooter drop ejector. Height restrictions formed by the cavity in the base prohibited the drop ejector from attaining proper clearance between the ejector nozzle and the substrate.

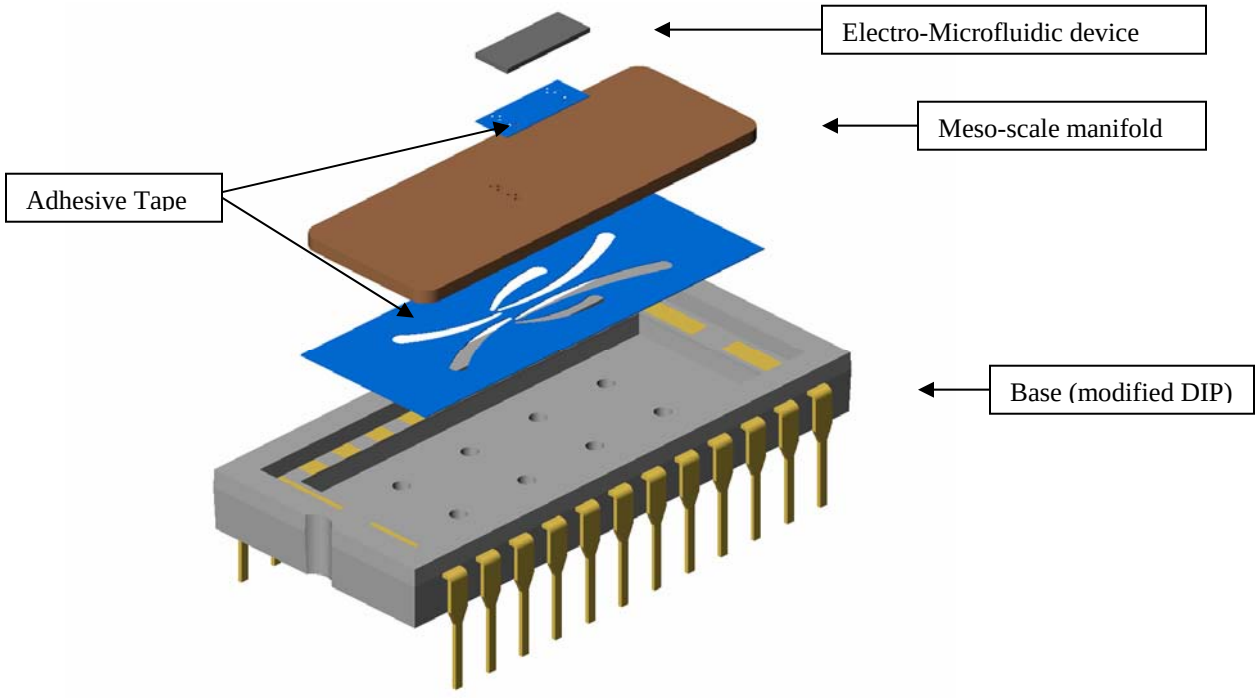

Figure 21: Exploded view of the 24-pin, 8-channel EMDIP™.

Our solution to the clearance height issue posed by the sideshooter drop ejector was to simply place the meso-scale manifold, contained within the modified DIP, directly on the FPWB. The modified DIP would no longer be needed. Therefore, our attention focused on how to place electrical traces onto the meso-manifold and how to properly align it with the FPWB. The same technique used to produce the electrical traces on the cover board would be used on the meso-manifold, just on a much smaller scale. This new meso-manifold is shown in Figure 22. The electro-microfluidic device will be contained within the wire bond pads located in the center of the manifold and aligned with the eight through holes. The machined channels shown on the right side in Figure 22 represent the current design configuration for the sideshooter drop ejector, but can easily be machined to accommodate a wide variety of devices. The eight through holes slightly visible on the left side in Figure 22 are 150 microns in diameter.

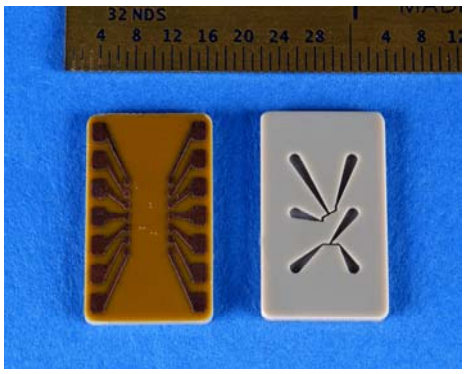

Figure 22: Top and bottom views of meso-manifold.

Manufacturing and Assembly Process:

The manufacture and assembly of the electro-microfluidic package is completed in stages. First, copper is laminated onto a large 1mm thick sheet of PEEK to produce the electrical traces needed for the cover board and meso-manifold. The cover board and meso-manifold are each 1mm thick. Copper is laminated onto PEEK using an adhesive film, Pyralux. Pyralux comes in two distinct forms, flame retardant and copper clad, each with thickness ranging from 1mil to 5mil. The chemical and mechanical properties remain the same for both forms; however, the flame retardant Pyralux film does not yield a 'burnt' surface when subjected to an elevated temperature. Since most of the copper will be etched away, exposing the Pyralux film, the flame retardant form is used in the lamination process. Several experiments were conducted to

best determine the temperature and pressure and thickness of film needed to successfully laminate copper onto PEEK. It was concluded that two 1mil sheets of fire retardant Pyralux film sandwiched between 10mil copper and 40mil PEEK for 90 minutes at a temperature of 375°F and a pressure of 400psi formed the strongest bond.

The entire copper laminated sheet is then patterned with multiple cover board and meso-manifold designs and chemically etched to expose the copper traces. Once the copper is etched away exposing the electrical traces, each individual pattern is then machined to produce cover board and meso-manifold 'blanks'. These blanks can then be machined per package requirements. This process is outlined in Figure 23 below.

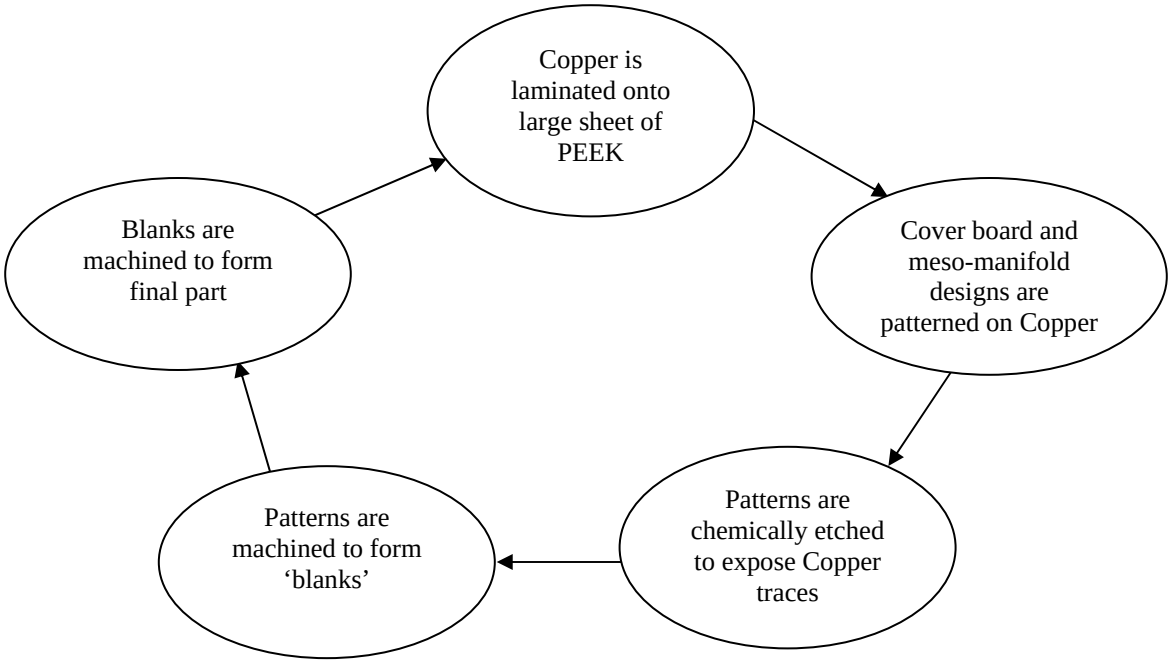

Figure 23: Outline of cover board and meso-manifold manufacturing process.

The second stage in the manufacturing process is to machine the channel board. The channel board contains the fluidic channels and threaded flat-bottom ports needed to make the fluid connections to the meso-manifold. The channel board is 5mm thick and machined out of PEEK. There are six individual fluid channels in the channel board and are designed such as to eliminate stagnate fluid build-up and minimize dead volume. The channels shown in Figure 20 are 1mm across and 2mm deep. In addition, there are four #6-32 threaded holes located on the underside of the channel board that may be used for mounting to larger, third level packages.

The electro-microfluidic package is assembled in layers using Pyralux adhesive film. The Pyralux film will be used to bond PEEK to PEEK in addition to Copper to PEEK. The first stage in assembly is to bond the cover board to the channel board. Six 1mm dowel pins will be used to align the channels in the channel board to the through holes in the cover board. Two 1mil sheets of Pyralux, machined with the same footprint as the channel board, will be placed between the two package components and aligned using the dowel pins. Once the channel board and cover board have been properly aligned, with Pyralux film sandwiched in between, the dowel pins are removed and the assembly is carefully placed in an oven. The oven is heated to 375°F and a pressure of 400psi is applied to the cover board. It takes approximately 1 hour 30 minutes to successfully bond PEEK to PEEK at these settings.

Once the FPWB has been assembled, our focus turns toward attaching the electro-microfluidic device to the meso-manifold. The attachment may be completed using a variety of adhesives including Pyralux film and 3M VHB transfer adhesive tape. However, to reduce the risk of fluid contamination the Pyralux

adhesive film is the preferred method of attachment. In addition to having exceptional fluid compatibility characteristics, Pyralux also maintains other advantages over transfer tapes. Since Pyralux is somewhat of a cross between a thermoset and thermoplastic adhesive it has the ability to re-flow under certain conditions. This unique characteristic becomes favorable when trying to attach the electro-microfluidic device to the meso-manifold. In particular, in the manufacture of the meso-manifold, once the copper is chemically etched away, a layer of Pyralux is exposed. This layer will then be used to attach the device to the meso-manifold. This eliminates the need to machine the adhesive with the same meso-manifold hole footprint where the features are on the order of 100 microns. While utilizing the re-flow properties to Pyralux is of substantial benefit, further testing is needed to determine actual feasibility. A flip-chip alignment system is used to align the electro-microfluidic device to the meso-manifold and then used to attach the device to the manifold. The flip-chip alignment system allows very tight tolerance alignment, down to 1 micron (0.00004 inches). Figure 24 shows the electro-microfluidic device attached to the meso-manifold using Pyralux adhesive re-flow characteristics.

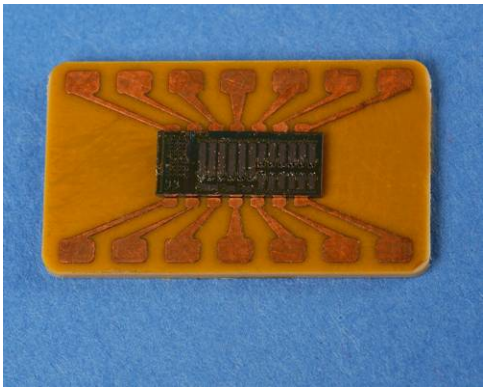

Figure 24: Meso-manifold with electro-microfluidic device attached.

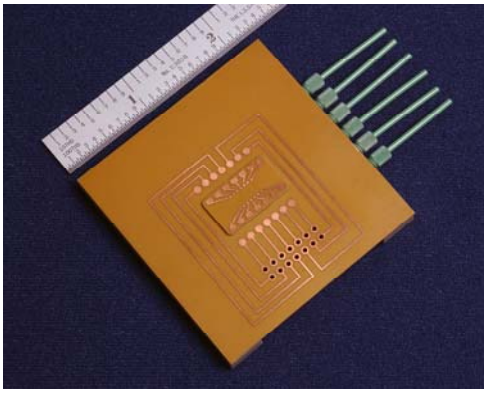

Figure 25: Fluidic Printed Wiring Board (FPWB) with meso-manifold and fluid connectors attached.

Once the electro-microfluidic device has been successfully attached to the meso-manifold, the flip-chip alignment system is then used to attach it to the FPWB. Once again, Pyralux re-flow characteristics may be used to attach the meso-manifold to the FPWB. The Pyralux adhesive film layer, exposed after the copper is etched away on the cover board, may be used at this interface. Other adhesives, including double sided VHB adhesive transfer tape, may also be used at this interface. Figure 25 shows the meso-manifold and six standard fluidic connectors attached to the FPWB. Wire bonding is used to make the electrical connections from the meso-manifold to the electro-microfluidic device and from the FPWB to the meso-manifold. The standard ribbon connector, shown in Figure 1.1, is attached using solder bonding.

It is important to note that in addition to using Pyralux to bond PEEK to PEEK, thermal bonding of PEEK was also considered. This approach eliminates the need to apply an adhesive at the interface, enhancing the chemical resistance of the package while simplifying its manufacture. Several experiments were used to determine the feasibility of creating embedded channels using thermal bonding. While significant progress was made in the thermal bonding of PEEK to PEEK, the results of these experiments suggest that bonding PEEK directly to PEEK is not a feasible method to create embedded microfluidic channels. The primary difficulty in hot welding semi-crystalline polymers is achieving adequate bondline strength while maintaining dimensional control. Achieving adequate bondline strength requires processing the polymer above its melt temperature, while dimensional control is maintained if the polymer is processed below its melt temperature. Thus, direct bonding of PEEK is best suited for creating solid parts in confined geometries.

Vision and Motion System

The 3rd key subsystem required for our solution based MEMS drop ejector fabrication system is the motion control and vision system. This system is needed in order to position ejected drops relative to each other over a larger scale than is possible with drop ejection control and thus produce a desired material pattern.

The machine vision and motion control system hardware consist of a motion controller, three high-precision (<1µm accuracy) stages for movement in the X, Y, and Z directions, a high-resolution digital camera, and an image acquisition PC card. All the hardware is computer-controlled and interfaced through LabVIEW.

The entire motion system is manufactured by Aerotech. The motion controller, named Npaq, is a 3U high, 19" rack-mount chassis capable of powering up to six axes of motion. It connects to the host PC using a high-bandwidth Firewire interface. This eliminates the need for a motion control card, and allows for complex, synchronized motion to be very deterministic. In a microsystem format this controller would be miniaturized. The controller contains three digital amplifiers that run the three motion stages. Motion in the X and Y directions are handled by Aerotech's ANT-25L nano-translational stages. These stages are best-in-class for combining speed, accuracy, resolution, repeatability, reliability, and size. They perform with a resolution of less than 10 nm and a stroke of 25 mm. The stage for motion in the Z direction is an Aerotech ATS-100. The ATS-100 provides exceptional stiffness and stability for high loads, while maintaining precision performance in a compact package. It has a resolution of 0.5 µm with a stroke of 50 mm.

The motion system can be controlled and programmed in native RS-274 G-code, C, C++, VisualBASIC, or LabVIEW languages. LabVIEW was used for the vision application because of its ease of integration with the other vision components like the camera system. LabVIEW programmatically accesses the motion controller by making function calls to C++ library functions contained in an Aerotech .dll.

The machine vision system incorporates a high-resolution digital camera, a PC image acquisition card, and a software toolkit for programming machine vision applications. The digital camera is a Hitachi KP-F100BCL that features a high-grade, progressive scan monochrome CCD with 1392x1040 effective square pixels and a Camera Link interface for simple cabling. The image acquisition card is a National Instruments PCI-1428 which combines high-resolution and high-speed image acquisition for Camera Link cameras.

The PC which controls all the motion and vision hardware, along with running the vision software also contains a National Instruments National Instruments PCI-6733 high speed voltage output PC card. This card is used to trigger the small servo-actuator system of the drop ejector. In the integrated system the trigger would also be used to control the voltage signal to the MEMS drop ejector causing a drop to be produced at the right time for the desired pattern. The card is programmed and triggered with LabVIEW for easy integration into the vision software.

The vision software is derived from a suite of programming tools contained in the Vision Development Module from National Instruments. Using these tools along with LabVIEW as the programming language, various machine vision applications can be implemented and coordinated with all the current hardware. These applications include inspection, pattern matching, color matching, gauging, particle analysis, alignment, and OCR.

The vision software for the drop ejector project was designed to use pattern matching for alignment of a MEMS device under the drop ejector for precision placement of the drop. The fixture for any MEMS device on the motion stage can not consistently hold every similar MEMS device in the same orientation. However, the on-chip features of a MEMS device always have the same orientation relative to each other because of their manufacturing process. Pattern matching allows the program to determine exactly what orientation the on-chip features of a MEMS device is in, and then apply an adjusted coordinate system to the current orientation. Once the new coordinate system has been determined, the software can then

accurately measure the distance to any on-chip region of interest. The straight-line distance is broken up into its vectors in the X and Y directions which can be sent to the motion controller to accurately position the stages.

Pattern matching and gauging is implemented in the program by training the software with a few images. The first image that must be trained is an image of a highly accurate calibration grid of black dots purchased from an optics supplier. This grid will calibrate the software and allow it to accurately convert pixel coordinates into real-world coordinates for measurements.

The second image or images that must be trained are the images used for pattern matching. These images serve as a template for the pattern-matching algorithm. Several factors are critical in creating template images; including, symmetry, feature detail, positional information, and background information. Once a good template image is trained, the pattern matching algorithm can detect the following items in an inspection image: the pattern in the image, the position of the pattern in the image, the orientation of the pattern, and multiple instances of the pattern (if applicable).

Below is an example of an implementation of the pattern-matching software. The inspection image is shown in Picture 1. Two patterns are trained, one pattern to define the on-chip coordinate reference (Picture 2a), and one pattern to find a point of interest (Picture 2b).

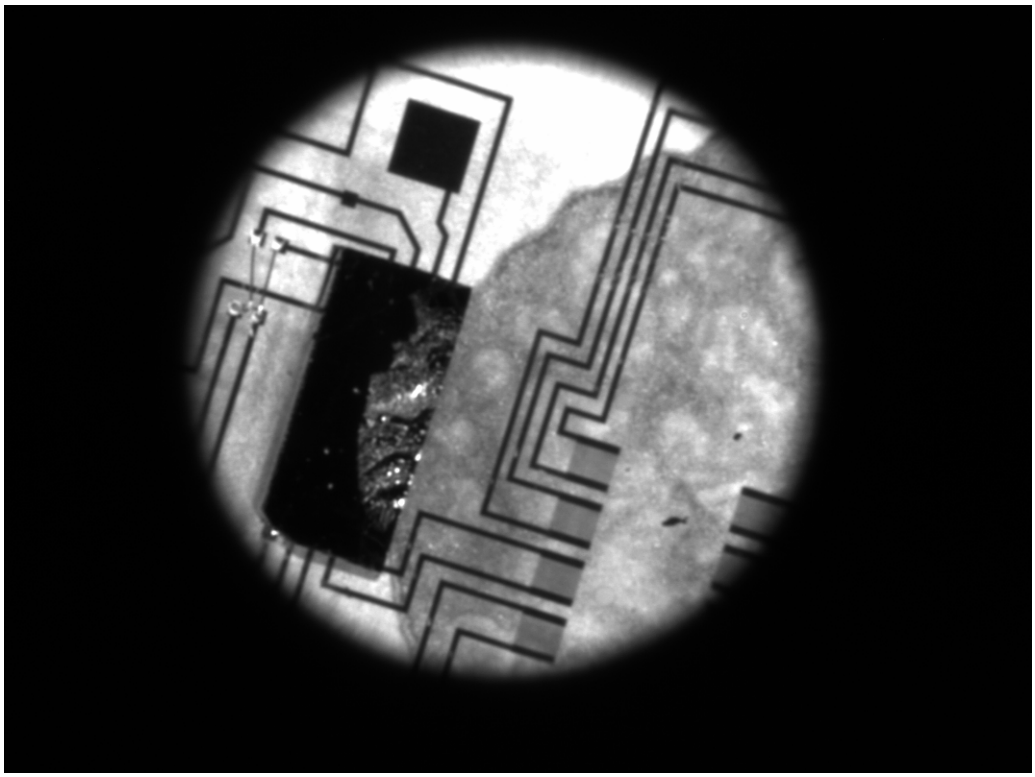

Picture 1

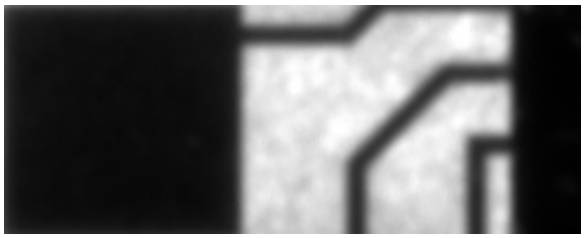	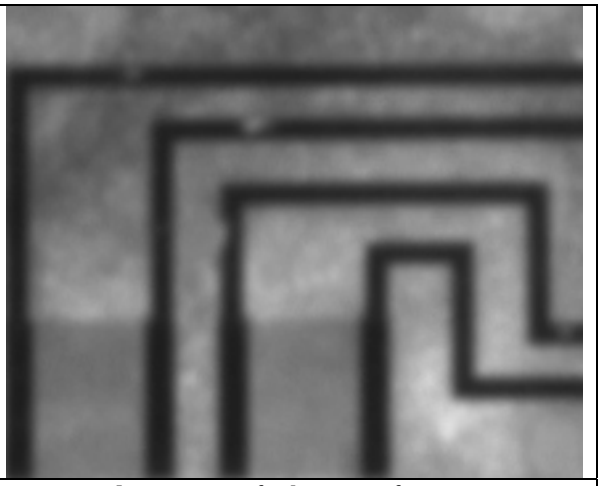
2a. Pattern to find new Coordinate Reference	**2b**. Pattern to find region of interest

The program can find the pattern in 2a and create a new coordinate reference at its location. Then, it can find the pattern in 2b as a region of interest. Pixel measurements of its distance from the new coordinate reference can then be converted to a real-world measurement. The results are visually demonstrated in Picture 3. Of course, the region of interest could be anything from the center of the camera to a micro-drop. Also, the measurements taken can be used for inspection purposes, or creating the offsets to move the stages.

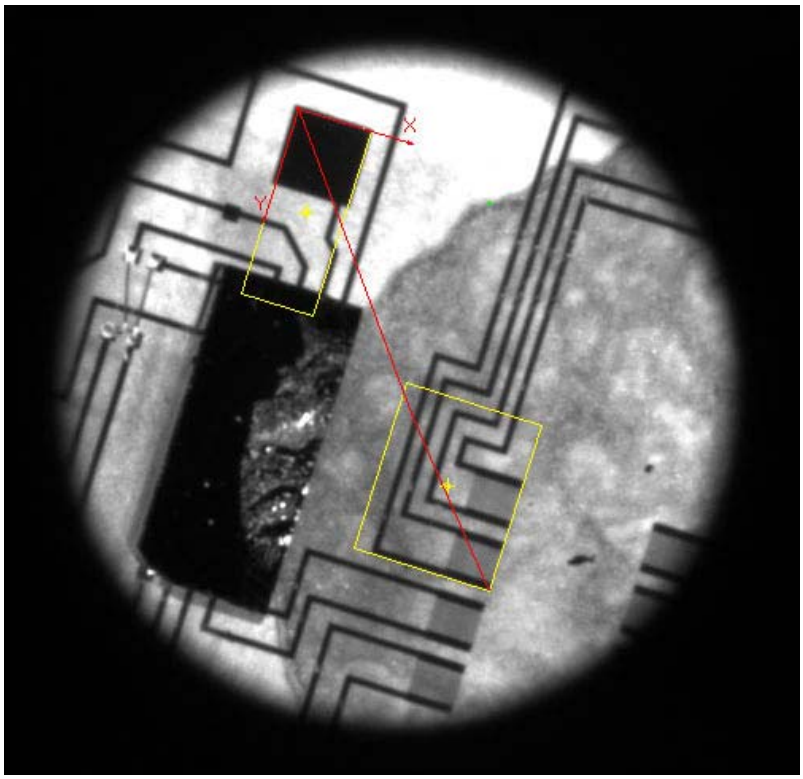

Picture 3

Conclusions and Further Work

In this LDRD we have successfully demonstrated the operation of the 3 critical subsystems required for the development of a droplet based MEMS sideshooter nano-microfabrication system: (1) the MEMS sideshooter ejector, (2) an effective package and system configuration, and (3) the vision and stage motion control system. The next step is to integrate these components into a working microfabrication system.

To make the first level system demonstration we need to do the following:

(1) Assemble anticipated working die with new ejector package and eject drops in ejector test station
(2) Take working packaged ejector to stage/vision system and eject a simple ink pattern of 8 micron diameter drops onto paper.
(3) Eject DNA solution in a pattern on glass or some other application of interest (e.g. pattern a SAW sensor with and absorbing coating of interest to the chem.-lab group).

The next level of future work toward making a system that might have commercial and national security uses is to demonstrate some of the unique capabilities of this system with a new more capable ejector design in the package and patterning system – with any needed changes to the package and patterning system uncovered in the first level demonstration described just above. The unique patterning capablilities we should attempt to demonstrate could include:

(1) Array of different drop sizes – down to 1 micron drops – try out thermal actuators and new seal designs.
(2) Different drop materials from same module of ejector designs.
(3) Different viscosity (and other property) liquids ejected
(4) Mix-then-eject
(5) Drop direction control
(6) One micron precision
(7) Quasi-3D pattern formation

References

1. Lee J-D, Yoon J-B, Kim J-k, Chung H-J, Lee C-S, Lee H-O, Lee H-J, Kim C-K, Han C-H, "A Thermal Ink-jet Printhead with a Monolithically Fabricated Nozzle Plate Self-Aligned Ink Feed Hole", Journal of Microelectromechanical Systems (JMEMS), Vol. 8, No. 3, September 1999.
2. Forrest S R, "The Path to Ubiquitous and Low-cost Organic Electronic Appliances on Plastic", Nature, Vol. 428 29 April, 2004.
3. de Heij B, van der Schoot B, Bo H, Hess J, de Rooij N F, "Characterization of a fL droplet generator for inhalation drug therapy", Sensors and Actuators 85 (2000), pp 430-434.
4. Demers L M, Ginger D S, Park S-J, Li Z, Chung S-W, Mirkin C A, "Direct Patterning of Modified Oligonucleotides on Metals and Insulators by Dip-Pen Nanolithography", Science Vol 296, 7 June 2002, pp. 1836-1838.
5. Ekstrom S, Ericsson D, Onnerfjord P, Bergtssom M, Nilsson J, Gyorgy M-U, Lannell T, "Signal Amplification Using 'Spot-on-a-chip' Technology for the Identification of Proteins via MALDI-TOF MS", Analytical Chemistry Vol 73, No 2, January 15, 2001.
6. Lipsker D, "Rapid Prototyping", US Patent 6,153,034 November 28, 2000.
7. Tanyeri M, Kennedy I M, "Microdroplets for integrated high sensitivity biosensors", Proceedings of SPIE Vol. 5275, BioMEMS and Nanotechnology (2004), pp. 133-140.
8. Fan H, Lu Y, Stump A, Reed S T, Baer T, Schunk R, Perez-Luna V, Lopez G P, and Brinker C J, "Rapid prototyping of patterned functional nanostructures", Nature, Vol. 405, 4 May 2000.
9. Gooray A, Roller G, Galambos P, Givler R, Zavadil K, Peter F, "Design of a MEMS Ejector for Printing Applications", Journal of Imaging Science and Technology, Vol. 46, Number 5, September/October 2002.
10. Ballantine D S, White R M, Martin S J, Ricco A J, Zellers E T, Frye G, Wohltjen H, Acoustic Wave Sensors, Academic Press 1997.
11. Rodgers M S, Kota S, Hetick J, Zhe L, Jensen B D, Krygowski T W, Miller S L, Barnes S M, Burg M S, "A New Class of High Force, Low-Voltage, Compliant Actuation Systems, Solid State Sensors and Actuators Workshop, Hilton Head SC, June 4-8 2000.
12. Shunk P R, Sackinger P A, Rao R R, Chen K S, Cairncross R A, Baer T A, Labreche D A., "GOMA – A Full-Newton Finite Element Program for Free and Moving Boundary Problems with Coupled Fluid/Solid Momentum, Energy, Mass and Chemical Species Transport: Users Guide", SAND-2404, September 1988.
13. Rick Givler (dept. 9114), personal communication.
14. Bosch Patent No. 5501893:"Method of Anisotropically Etching Silicon", Robert Bosch Gmblt, Issued 1996.
15. SAND2002-1941, "Electro-Microfluidic Packaging", Gil Benavides and Paul Galambos.

Distribution:

1	MS1080	Paul C. Galambos	1769
1	MS1080	David Luck	1769
1	MS1080	Ken Pohl	1769
1	MS0958	Gil Benavides	14132
1	MS0958	Mark Braithwaite	14132
1	MS1003	Clint Atwood	1314
1	MS0834	Rick Givler	9114
1	MS0834	Joel Lash	9114
1	MS1415	Dave Czaplewski	1112
1	MS1415	Paul Dressendorfer	1116
1	MS1073	Steve Rohde	17382
1	MS1080	Sita Mani	1749
1	MS1080	Amanda Lopez	1749
1	MS1080	Jamie Reif	1769
1	MS0958	Guy Prevost	14153
1	MS0603	Randy Shul	1763
1	MS0603	Sarah Rich	1763
1	MS1310	Bernie Jokiel	1745
1	MS0892	Susan Brozik	1744
1	MS1349	Hongyou Fan	18431
1	MS1349	Jeff Brinker	1002
1	MS1073	Ron Anderson	17382
1	MS1073	Dave Peterson	17381
1	MS0892	Pat Lewis	1764
1	MS0886	Jeri Timlin	1812
1	MS0886	David Haaland	1812
1	MS1080	David R. Sandison	1769
1	MS1077	Thomas Zipperian	1740
1	MS1071	Jerome Jakubczak	1703
1	MS1078	Steve Martin	1707
1	MS0892	Joe Simonson	1764
1	MS0892	Richard Cernosek	1764
1	MS1454	Alex Tappan	1454
1	MS 9018	Central Technical Files	8945-1
2	MS 0899	Technical Library	9616
1	MS 0323	D. Chavez, LDRD Office	1011